Experimental Modelling of Fragmentation Processes within Phreatic and Hydrothermal Eruptions

A thesis submitted in partial fulfilment of the requirements for the Degree of Master of Science in Geology

at the University of Canterbury

By Lauren Charlotte Foote

University of Canterbury

2012

Frontispiece

The 700 year old explosion crater, Lake Okaro, looking north-east to Mount Tarawera – February 2011

Table of Contents

List of Figures

Acknowledgements

This thesis was completed with the help and support of many people. Firstly thanks to all my supervisors for coming up with such an interesting and exciting project. Without realising it you combined two of my favourite things – water and volcanoes, to creating the perfect project!

Thanks to all the technical staff in the department, I would never have finished this without your help. Thanks to Kerry for helping me with everything after the earthquake, Rob for making my thin sections and helping with my permeability trials, Chris for helping find or make equipment when ever I needed it, Cathy and Vanessa for all your help in the lab and Sacha for sorting things out whenever I needed extra help.

For funding a big thank you goes to the Mighty River Power Source to Surface scholarship for covering the majority of costs associated with this project. Thanks to LMU for funding my accommodation while in Munich and the use of your labs. Additional thanks to those that provided funding for me to attend the AGU conference: Royal Society of New Zealand – Canterbury Branch, Canterbury Federation of Graduate Women, Mason Fund and again the Mighty River Power Source to Surface scholarship.

To everyone I met while travelling, at conferences and courses thanks so much for all the great times, new ideas and encouragement. I would especially like to thank those of you that managed to help me source unpublished papers and reports, these added many useful details to this thesis.

Extra thanks go to Jim Cole for reviewing my thesis before hand in.

Thanks to all the students within the geology department (both at Canterbury and LMU) - we had so many good times and adventures along the way! Big thanks to everyone that shared 401 with me, you guys rock!

Finally thanks to my family for all your encouragement and support through my whole university career, I would never have made it this far without your help.

Thesis Abstract

Phreatic and hydrothermal eruptions often occur with little or no warning representing a significant hazard within geothermal regions. These violent eruptions occur at a range of temperatures and pressures within varying rock types. A range of mechanisms including heating or decompression, allows hydrothermal/supercritical fluid to rapidly flash to steam, expanding and shattering the surrounding rock to produce an eruption, with no direct magmatic influence.

These eruptions are highly variable resulting in the current wide ranging classification schemes, many of which are based on characteristics that are hard to observe and define. This has resulted in confusing nomenclature with many different terms used to describe the same eruptive phenomena. Here a new classification scheme is presented, based on the easily definable features of eruption size, trigger type (natural or anthropogenic) and geological setting (volcanic or hydrothermal). This ultimately produces a classification dividing the eruptions into either phreatic, where magma interacts with cold water but no juvenile material is erupted; or hydrothermal where eruption occurs from an already heated hydrothermal system. Examples are then provided for each classification type.

Previous studies have focused exclusively on either physical characteristics of eruptions, small scale experimental modelling of trigger processes or mathematical modelling of various eruption characteristics. Here, a new experimental procedure has been developed to model phreatic fragmentation, based on shock tube experiments for magmatic fragmentation by Alidibirov and Dingwell (1996). Water saturated samples are fragmented from a combination of argon gas overpressure and steam flashing within vesicles. In this thesis, these experimental results have been integrated with the physical characteristics of porosity, permeability and mineralogy to create two new models of phreatic fragmentation. Firstly a generalised model to explain fragmentation processes and secondly a specific model describing the eruption forming Lake Okaro, within the Taupo Volcanic Zone of New Zealand. These models were developed with the overall aim to improve understanding of these eruption types, ultimately improving future hazard modelling.

Experiments were performed on Rangitaiki ignimbrite, through which the Okaro eruption occurred. In order to evaluate alteration effects, both unaltered ignimbrite and hydrothermally altered ignimbrite samples were analysed. Experiments were performed at room temperature and 300°C with pressures from 4 to 15 MPa, to reflect likely geothermal conditions while also assessing the effect of liquid water on fragmentation.

Results indicate that within these samples 5 to 8 MPa of decompression is required to trigger an eruption, fitting well with the previously identified trend between decompression and porosity for magmatic samples. The fragmentation front propagates through the sample at speeds ranging between 14 m/s to 42 m/s, increasing with higher applied pressures and higher sample porosity. Most importantly, grain size analysis from these experiments show a clear shift to smaller grain sizes when liquid water flashes to steam (independent of pressure or sample type), reflecting the greater energy involved with steam flashing. Previous grain size analysis of the Okaro breccia deposits have indicated that the highest weight percentage of fragments fall between -3.5 and 1.5 phi, with our experimentally produced fragments fitting right within this range at -0.5 to 1.0 phi.

Here the first parameterisation of conditions for phreatic and hydrothermal eruptions is presented creating a general fragmentation model along with a case study on Lake Okaro. These models describe how eruptions occur, with stages from initial system priming and overpressure development through to the last stages of eruption and crater formation.

Chapter One

Introduction and Review of Current Knowledge

1.1 Overview

Phreatic and hydrothermal eruptions are common forms of volcanism within geothermal fields around the globe (Browne & Lawless, 2001; Smith, 2000; Smith & Mckibbin, 2000; Mastin, 1995). Both represent forms of explosive volcanism driven by the expansion of vapour when water flashes to steam (Morgan et al., 2009), driven by rapid decompression or heating (Buttinelli et al., 2011). Magma is not involved in either eruption although may be present at depth (Germanovich & Lowell, 1995). Erupted material is composed entirely of fragmented underlying lithologies, ranging in size from large blocks down to fine ash (Barberi et al., 1992). Although common, these eruptions are still poorly understood; largely due to their unpredictable nature and lack of precursor signals (Bromley & Mongillo, 1994; Barberi et al., 1992). As a result most eruptions occur with little to no warning creating a significant hazard for both natural and anthropogenic features nearby (Morgan et al., 2009). Improved knowledge of the mechanics of these eruptions is essential to improve hazard and risk assessment.

Trigger mechanisms are usually attributed to some aspect of rapid decompression or heating. Triggering can occur as a result of large scale processes such as earthquakes, landslides, draining of lakes (Browne & Lawless, 2001; Barberi et al., 1992; Muffler et al., 1971) or by more subtle processes such as a drop in atmospheric pressure or a slight change in the heat supplied to the system (Bixley & Browne, 1988; Nelson & Giles, 1985). Since development

of the geothermal industry, anthropogenic triggers can produce these eruptions. Decompression resulting from either geothermal exploration or production drilling can produce eruptions, presenting a significant risk to site workers and infrastructure (Bixley & Browne, 1988; Hedenquist & Henley, 1985).

It is important to measure the pressures required, the energies involved, the speed of fragmentation, and the resultant grain sizes, to aid future predictions of when and where eruptions may be triggered. Previous attempts to understand their operation have focused exclusively on either studies of physical characteristics of eruption deposits (Hedenquist & Henley, 1985; Collar & Browne, 1985; Morgan et al., 2009) or modelling of the eruption processes. Both mathematical (Fullard, 2011; Mastin, 2001; Smith & Mckibbin, 2000; Thiéry & Mercury, 2009) and experimental (Dellino et al., 2010; Fowler et al., 2009) modelling has been conducted providing valuable information on how these eruptions operate.

1.2 OUTLINE OF THESIS STRUCTURE

Chapter 1 introduces the subject, the previous literature, proposes a simplified classification scheme based on type examples and also describes the overall project aims. Chapter 2 forms a publishable paper in preparation for submission to the Journal of Volcanology and Geothermal Research. Collaboration with co-authors (Bettina Scheu, Ben Kennedy and Darren Gravley) was required for additional expertise in data analysis and/or collection of data, ensuring the development of sound interpretations prior to the manuscripts submission. Overall this chapter describes the experimental study completed to produce a generalised model for both phreatic and hydrothermal eruptions. Chapter 3 expands the work in 2, detailing a specific eruption at Lake Okaro, within the Taupo Volcanic Zone of New Zealand.

1.3 PROJECT AIMS AND OBJECTIVES

This study focuses on experimental modelling of phreatic and hydrothermal eruptions, using natural breccia samples from a 700 year old eruption crater. This material was chosen to constrain the natural parameters influencing how these eruptions occur. To improve upon the knowledge gained from previous studies, here their work is integrated with a field study and

experimental results, with the overall aim of providing information for future hazard models. To do this the main objectives are:

1. Characterise the sample material in terms of key factors influencing fragmentation. This includes mineralogy, density and porosity.

2. Determine the key fragmentation parameters for two main eruption types – those that are driven by gas expansion and those driven by steam flashing.

3. Measure grain size distributions for these two eruption types in order to compare the fragmentation efficiency.

4. Develop a model illustrating how fragmentation occurs within phreatic and hydrothermal systems.

1.4 HYDROTHERMAL AND PHREATIC ERUPTIONS

Nomenclature to describe various hydrovolcanic systems has been used with widely different meanings from publication to publication (Barberi et al., 1992; Browne & Lawless, 2001; Germanovich & Lowell, 1995; Smith, 2000; Fullard, 2011; Hardy, 2005). Classifications have been developed based on different characteristics including fluid types, temperatures, amount of debris and the cause of eruption (Smith, 2000). In many cases these factors cannot be clearly defined, leading to the wide variety of names for the same eruption types. These include phreatic, hydrothermal, steam blast, boiling point, and hydro-explosions among many others (Barberi et al., 1992; Smith, 2000). As a result of these inconsistencies, definitions should always be clearly stated to avoid confusion. Here the properties of phreatic and hydrothermal eruptions are discussed, before development of a new and simplified classification scheme based on easily defined characteristics.

A key factor of these eruptions is that no juvenile material is erupted, therefore leading to the term “non-juvenile eruptions” (Mastin, 1995). To further define phreatic and hydrothermal eruptions, only those that result from flashing of water or supercritical fluid to steam, caused by either rapid decompression or heating are considered. Again definitions for these two eruptions vary significantly, with some authors suggesting cold or hot water sources to differentiate the two (Browne & Lawless, 2001), with others suggesting meteoric or

hydrothermal as the difference (Smith, 2000), with many variations on this. This research does not focus on the differences; it only considers the processes occurring after triggering, when fragmentation of either eruption type behaves the same way. In both cases explosions and eruptions occur. The term explosion is indicative of short bursts of activity involving single blasts lasting for seconds to minutes, while eruptions indicate longer phases of activity with repeated explosions lasting from minutes to hours (Smith, 2000).

Fragmentation will occur only when the pressure within the system exceeds that of the tensile strength of the surrounding rock, in addition to lithostatic and hydrostatic pressures (Nelson & Giles, 1985). Within phreatic and hydrothermal systems this is driven by steam flashing or expansion which converts thermal energy to mechanical energy, providing the necessary energy to shatter the overlying rock, ultimately producing an explosion (Browne & Lawless, 2001; Montalto, 1995). Eruption will continue as long as there is expansion occurring to drive the eruption, so duration is strongly dependent on the amount of water or steam within the aquifer (Handal & Barrios, 2004).

1.4.1 Eruption and Deposit Characteristics

Although explosive, these eruptions are much smaller than their magmatic counterparts (Montalto, 1995). Individual explosive events may be very short lasting from seconds through to longer events lasting up to several hours (Buttinelli et al., 2011; Smith, 2000). Based on current observations, the average plume heights reach up to 100 m (Figure 1.1), with several exceptions where larger eruptions have produced plumes up to several hundred meters (Browne & Lawless, 2001). These eruptions produce craters ranging in size from just a few meters through to craters more than 2 km in diameter (Morgan et al., 2009).

Figure 1.1: Steam plume from the 2005 Ngatamariki eruption, photo courtesy of Bruce Mountain, GNS Science.

Early estimates of eruption initiation depths suggested that they occurred at relatively shallow focal depths of less than 450 m (Browne & Lawless, 2001). Recent studies have suggested that they may reach much greater depths. A study of Baccano Crater, Italy, provides evidence to suggest that at this location the eruption may have been initiated at depths as great as 1.2 km (Buttinelli et al., 2011). With any eruption, initiation depth is difficult to determine. During eruption, craters are instantly filled as material falls back and slumping occurs, therefore crater depths are not representative (Smith & Mckibbin, 2000). Crater depth can be estimated based on the volume of erupted material, combined with an approximate crater shape (Hedenquist & Henley, 1985). Alternatively, clast types within the eruption breccia can be used to identify the stratigraphically deepest unit, therefore suggesting a minimum excavation depth (Browne & Lawless, 2001). Along with these techniques, the presence of any hydrothermal alteration can be used as an indication of likely temperatures, suggesting potential depths at which the eruption occurred (Nogami et al., 2000).

Breccia deposits are composed entirely of lithics from the underlying stratigraphy, excavated during eruption, with no juvenile material and therefore no direct magmatic influence (Smith, 2000). Varying clast sizes from ash and mud through to large blocks measuring several meters in diameter, produce fall deposits thinning rapidly from source (Browne & Lawless, 2001). Extent is variable ranging from small deposits over a few square meters through to much larger eruptions over many square kilometres, such as the prehistoric Rotokawa

eruption which produced deposits over an area of 15 km^2 (Collar & Browne, 1985). During eruption, material can be fragmented and ejected repeatedly falling back into the crater, producing well mixed, poorly sorted deposits with no vertical lithologic sequence (Browne & Lawless, 2001; Morgan et al., 2009). These matrix supported deposits commonly contain clasts showing hydrothermal alteration and silicification reflecting the conditions within the hydrothermal system prior to eruption (Nelson & Giles, 1985).

1.4.2 ERUPTION PROCESSES

1.4.2.1 *PRECURSORS*

Phreatic and hydrothermal eruptions are highly unpredictable, as they lack the common precursors of other eruptions (Bromley & Mongillo, 1994). This makes prediction very difficult as they can occur with little to no warning. In rare instances precursors have been noted including seismic activity, geochemical changes (recorded from fumaroles, springs or surface lakes) or ground deformation (Barberi et al., 1992). Precursors appear to be rare but this may simply be due to a lack of monitoring. Permanent monitoring is only located in active volcanic regions, such as Mount Ruapehu which despite the modern monitoring array showed no precursors prior to the 2007 phreatic eruption (Mordret et al., 2010). Of the different precursors, seismic activity is the most commonly reported. Unfortunately in most instances occurring immediately before the eruption, with the greatest recorded time span between precursor and eruption being only several hours (Barberi et al., 1992). Although the identification of precursors is useful for hazard mitigation, the short duration between activity and eruption means that little can be done to protect densely populated areas. With current understanding of these eruptions, they are spatially too unpredictable to determine suitable areas for monitoring, particularly within actively migrating geothermal fields. At this stage precursors still can't provide a useful aid to hazard mitigation (Bromley & Mongillo, 1994).

1.4.2.2 *PRE-ERUPTION AND TRIGGERING*

Not all hydrothermal systems will produce eruptions. Before an eruption can occur the system must be primed, pushing it close to the eruption point through the presence of fluid at boiling or near boiling conditions (Smith & Mckibbin, 2000). Eruption will be triggered when

pressures within the system exceed that of the lithostatic pressure plus the tensile strength of the overlying rock (Nelson & Giles, 1985).

Many different trigger mechanisms have been identified to produce these eruptions, all ultimately causing pressure change or heating to disrupt the equilibrium of the system (Montalto, 1995). Decompression can occur as a result of large scale material removal events such as landslides, or crater-lake break-out, through to smaller events such as changes in barometric pressure (Barberi et al., 1992; Browne & Lawless, 2001). Pressurization can be caused by decreased permeability (trapping gasses), degassing of shallow magma systems or dykes, which may additionally act to heat the system (Mastin, 1995; Nairn et al., 2004; Nelson & Giles, 1985). Heat can be transferred from deeper magmatic sources by deeply circulating geothermal fluids, while dykes can transport heat close to the water that drives the explosion. Within a shallow geothermal system even a minor change can be significant enough to trigger an eruption. Earthquakes and minor seismic activity are suggested to be the most common trigger of these eruptions as they produce pathways to move fluid or gasses through the system (Barberi et al., 1992; Bixley & Browne, 1988; Browne & Lawless, 2001; Smith, 2000).

As well as natural trigger process, anthropogenic activity can produce these eruptions. Decompression occurring as a result of geothermal drilling, for both exploration and production can act as a trigger (Bixley & Browne, 1988; Hedenquist & Henley, 1985; Mastin, 1995), creating a significant hazard for the geothermal industry worldwide. Within New Zealand, eruptions occurring as a result of drilling have occurred at both Wairakei and Tauhara (Browne & Lawless, 2001). Future work to improve understanding of the conditions required to trigger these eruptions, may make it possible to identify which systems are most at risk of eruption, and therefore how to best proceed with exploration and production.

1.4.2.3 *FRAGMENTATION ENERGY*

Hydrothermal and phreatic eruptions occur as a result of water changing volume. Pressure and temperature conditions determine the phase of the fluid thereby controlling whether critical fluid, steam flashing or gas expansion is the main driver of eruption. Greater energy is produced with steam flashing due to the volume increase associated with the phase change rather than pure gas expansion without a phase change (Browne & Lawless, 2001).

1.4.2.4 *ERUPTION MECHANISMS*

Various mechanisms have been proposed to describe how eruption occurs within phreatic and hydrothermal systems, all of which ultimately describe situations where the pressure within the system exceeds that of the overlying lithostatic pressure and tensile strength (Browne & Lawless, 2001). This can occur where a cap rock exists, trapping pressure in the system, followed by rapid subsurface pressure release allowing steam flashing to occur at depth; or with progressive flashing propagating down from the surface (Figure 1.2) (Browne & Lawless, 2001; Fullard, 2011).

Although either of these models may occur, boiling within the system (converting liquid water to vapour) will not occur until some trigger provides a depressurisation pathway. Thermodynamics dictate that the hydrothermal fluids can not boil until a fracture pathway is formed, allowing the fluid to migrate upwards to regions of lower pressure. If this migration occurs at fast enough rates it will shatter and lift the overlying rock, as long as the lithostatic and tensile strengths are overcome (Smith & Mckibbin, 2000).

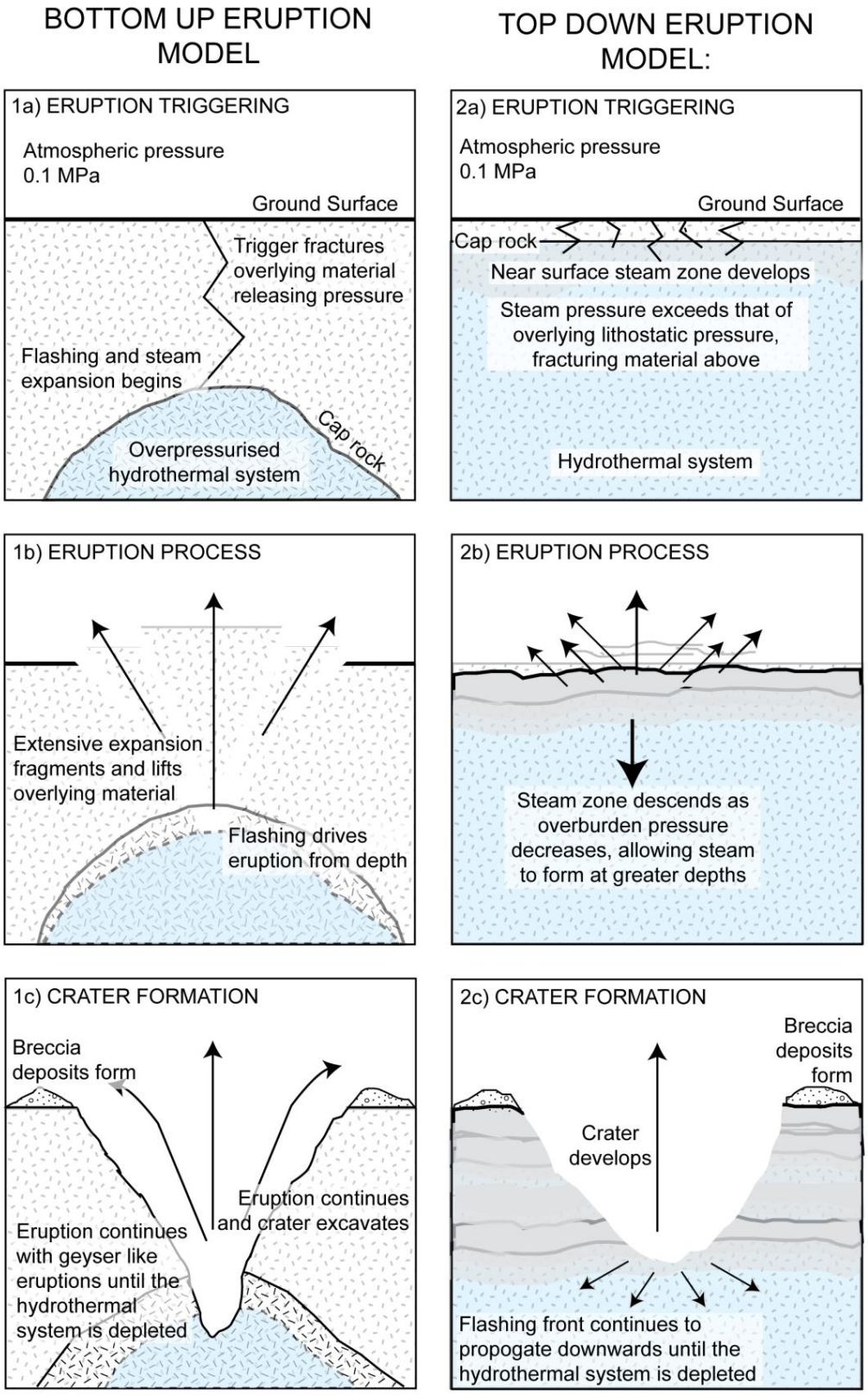

Figure 1.2: Simplified eruption models. Left (1a to 1c): bottom up mechanism, right (2a to 2c): top down mechanism, both illustrating the three main stages of eruption, triggering, eruption and crater formation.

1.4.3 Hazards

Geothermal fields are attractive regions for both tourism and industry, resulting in increased infrastructure and population in the areas most at risk of phreatic and hydrothermal eruptions. There are many hazards associated with this activity. Including falling blocks and debris, the release of toxic gasses and the production of base surges, lahars and directional blasts (Barberi et al., 1992; Montalto, 1995). The impact of these hazards is increased by the unpredictability of these eruptions. As they can occur frequently and without warning, the associated hazards represent a high risk relative to their eruptive volume, in contrast to magmatic eruptions, which are generally predicted prior to eruption allowing evacuation of the areas most at risk.

An example of the devastating nature of these eruptions is the Agua Shuca eruption of 1990 in El Salvador. This resulted in the death of 26 people leaving an additional 15 people injured simply as a result of falling debris (Barberi et al., 1992; Handal & Barrios, 2004). Apart from the obvious hazards of debris, additional hazards have been noted to cause significant deaths. At the Dieng plateau, Indonesia, phreatic eruptions commonly release carbon dioxide. An eruption in 1979 resulted in the death of 149 people along with many livestock and fish (Barberi et al., 1992). Unfortunately for many living in or around geothermal areas, currently phreatic and hydrothermal eruptions occur across extensive areas and occur too rapidly for monitoring to be an option. Hopefully with future understanding this can be improved and monitoring may become a viable option to reduce the risk of these common eruptions.

1.4.4 Induced Eruptions

Risk of eruption is particularly significant for the geothermal industry as any changes may disturb system equilibrium, triggering eruption. To mitigate the risk of induced eruptions it is important to investigate any previous activity and the presence of any near surface aquitards. This should be completed in addition to monitoring steam and fluid flow, steam emissions, near surface temperatures, groundwater levels and potential reductions in lithostatic load when overburden is removed (Bromley & Mongillo, 1994). Any changes to these factors may indicate adjustment of the geothermal system which can then lead to eruption.

Both drilling and reinjection can change the system significantly enough to cause an eruption. Drilling can release high pressure steam from depth, allowing it to migrate towards the

surface reaching shallower unstable aquifers. Reinjection is a risk if large amounts of hot waste water (above 100°C) are pumped back into the system as this can heat the ground water to boiling point and induce an eruption (Bromley & Mongillo, 1994).

Typically induced eruptions are small. Lasting only a few hours while creating small craters up to 50 m in diameter, they form from shallow initiation depths of only several meters (Bixley & Browne, 1988; Browne & Lawless, 2001). The Wairakei geothermal field of New Zealand has experienced several induced eruptions in the 1950's and 60's as part of early development. Casing problems led to the development of a small fumarole near one of the well heads which was followed by a significant eruption. Activity continued for the following ten months until mitigation measures were taken. A new well was drilled to meet the previous and then filled with cement, acting as a plug (Bixley & Browne, 1988). Luckily modern monitoring techniques and drilling practices have been improved with many explosions of this kind prevented.

1.4.5 PREVIOUS MODELLING METHODS

Previous studies modelling these eruptions have used a variety of techniques from ballistic analysis through to small scale replication of the actual eruptions and mathematical calculations of various eruption characteristics (e.g. Dellino et al., 2010; Fowler et al., 2009; Fullard, 2011; Mastin, 2001; Smith, 2000; Thiéry & Mercury, 2009). Early experimental modelling of fuel coolant interactions (FCI's) for industrial applications provided an analogue study of phreatic eruptions (Sheridan & Wohletz, 1983). FCI experiments investigate the explosive activity occurring when a hot "fuel" interacts with a lower temperature "coolant", resulting in vaporisation of these products ultimately leading to explosion when the pressure can no longer be confined. These early experiments focused predominantly on the energy production involved in these explosions, determining how different ratios of fuel to coolant interact to release different energy levels and their resultant grain sizes, shapes and sorting (Sheridan & Wohletz, 1983; Wohletz, 1983).

Recent studies of magmatic fragmentation (after Alidibirov & Dingwell, 1996) can also be applied to processes within phreatic or hydrothermal eruptions. These experiments are performed with argon gas as scaled down models, using either natural or analogue materials to define key characteristics of fragmentation and conduit flow. Experiments are

predominantly based on the shock-tube method developed by Alidibirov and Dingwell (1996), which the experiments performed in this study are based on, and the large scale experiments by Dellino et al. (2010). Shock tube experiments represent layer by later fragmentation (Alidibirov & Dingwell, 2000), and allow parameterisation of the resultant fragmentation speeds (Spieler et al., 2004), energy (Kueppers et al., 2006; Alatorre-Ibargüengoitia et al., 2010) and grain sizes (Spieler et al., 2003), while the large scale experiments provide an indication of the eruptive style (convective plume or collapsing column) based on grain size characteristics, pressure and conduit geometry (Dellino et al., 2010).

Numerical mathematical modelling has been completed to determine a wide variety of factors influencing these eruptions. Investigating everything from the rock parameters that allow fragmentation to occur (specifically rock strength and permeability) (Germanovich & Lowell, 1995), to thermodynamic conditions (Mastin, 1995; Thiéry & Mercury, 2009) right through to the influence of geothermal flow on boiling processes (Smith, 2000) and conditions necessary to trigger eruption initiation (Fullard, 2011).

1.4.6 Proposed Classification Scheme for Phreatic and Hydrothermal Eruptions

As previously discussed, many different eruption characteristics and processes exist, all of which invariably complicate this classification. The following classification scheme is proposed, based predominantly on eruption size (depth, breccia volume and crater diameter), trigger type and geologic setting. This produces the six eruption types identified below in Figure 1.3.

ERUPTION SIZE Excavation Depth Deposit Volume Crater Depth	Small < 20 m < 5,000 m^3 < 30 m			Medium 20 - 200 m 5,000 - 10^6 m^3 30 - 500 m		Large > 200 m > 10^6 m^3 > 500 m
TRIGGER TYPE	Natural		Induced	Natural		Natural
SETTING	Volcanic	Geothermal	Geothermal	Volcanic	Geothermal	Geothermal
EXAMPLE	White Island	Waiotapu	Kuirau Park	Ruapehu	Okaro or Ngatamariki	Rotokawa
	TYPE 1 (phreatic)	**TYPE 2** (hydrothermal)	**TYPE 3** (hydrothermal)	**TYPE 4** (phreatic)	**TYPE 5** (hydrothermal)	**TYPE 6** (hydrothermal)

Figure 1.3: Proposed classification scheme for phreatic and hydrothermal eruptions. Based on eruption size, trigger and location, including New Zealand examples of White Island (Cole et al., 2000; Houghton, 1991),Waiotapu (Simmons et al., 2004; Nairn et al. 2004; Hedenquist & Henley, 1985, Kuirau Park (Scott et al., 2005; Doherty, 2009; Fullard, 2011; Bromley, 2003), Ruapehu (Doherty, 2009; Kilgour et al., 2010; Mordret et al., 2010), Ngatamariki (Milicich & Reeves, 2009; O'Brien, 2010), and Rotokawa (Bixley & Browne, 1988; Browne & Lawless, 2001; Collar & Browne, 1985).

Here the mechanisms operating within both phreatic and hydrothermal eruptions are considered to be the same, with location being the only difference. Phreatic eruptions occur on active volcanoes, while hydrothermal eruptions occur within a geothermal setting. This implies different fluid temperatures between the two settings. Within a volcanic setting, phreatic eruptions occur where cold water interacts with magma providing additional heat only, with no erupted magma; while hydrothermal eruptions occur within already heated hydrothermal systems. As with any rule there are exceptions, here occurring when the two end members meet. Firstly, a volcano can be underlain by a hot geothermal field, where the eruption is driven by additional heat from a magmatic source. For simplicity this is classified as a phreatic eruption based on its location, for instance White Island or Ruapehu (Christenson, 2000; Houghton, 1991). Secondly, a geothermal field can be intruded by

magma where there are no active volcanoes. Again this is classified based on location, representing a hydrothermal eruption.

1.4.7 EXAMPLES OF NEW CLASSIFICATION TYPES

Worldwide phreatic and hydrothermal eruptions are common events within volcanic and geothermal regions. New Zealand is no exception to this, so case studies of the 6 different eruption types are discussed below, within the local New Zealand setting.

1.4.7.1 *TYPE 1 – WHITE ISLAND*

Type 1 eruptions are characterised by small, naturally triggered events occurring in a volcanic setting. The phreatic eruptions from White Island are a classic New Zealand example. White Island is an andesitic/dacitic strato-volcano located off the Bay of Plenty coastline (Figure 1.4). The island has experienced frequent phreatic eruptions as a result of the shallow, non-saline, groundwater system (Houghton, 1991). In between magmatic phases, phreatic eruptions occur intermittently forming the normal background activity levels (Cole et al., 2000). It is thought that these are triggered when small magmatic pulses travel towards the surface, degassing and providing the necessary heat for eruption (Cole et al., 2000).

Figure 1.4: Left - aerial view of White Island, Right - view north through the crater showing a mixture of phreatic, phreatomagmatic and magmatic deposits (Photos by GNS Science and Lauren Foote).

1.4.7.2 *TYPE 2 – WAIOTAPU*

Type 2 eruptions are small scale events occurring naturally within geothermal areas. The Waiotapu region represents the largest thermal area within the Taupo Volcanic Zone, containing well over 20 hydrothermal eruption craters (for instance Champagne Pool, Figure 1.5) (Simmons et al., 2004); including many small scale events representative of the type 2 style. It is thought that they formed within a period of widespread activity between 700 and 800 years ago, possibly associated with the Kaharoa eruptions from Mount Tarawera (Nairn et al., 2004; Simmons et al., 2004). The formation of a silica cap across the whole Waiotapu geothermal field, was thought to have been the cause of increased hydrostatic pressure, priming the system for eruption (Hedenquist & Henley, 1985). This led to the formation of many small craters between 5 and 10 m in diameter, occurring along the Ngapouri fault line, suggesting a strong structural control, and likely seismic triggers (Hedenquist & Henley, 1985). Unfortunately these small craters have very few deposits making them difficult to study and therefore very little is known about them (Hedenquist & Henley, 1985).

Figure 1.5: Champagne pool eruption crater at Waiotapu (photo from Wai-O-Tapu Geothermal Wonderland retrieved 23/03/12 from http://www.waiotapu.co.nz/photos/features/)

1.4.7.3 *TYPE 3 – ROTORUA AND KUIRAU PARK*

Type three eruptions represent small events that occur because of human activity within geothermal settings. The Rotorua geothermal field has been significantly altered at shallow depths between 30 to 200 m, resulting in many hydrothermal eruptions (Scott et al., 2005). A strong correlation exists between phases of significant change to the geothermal system and increased numbers of hydrothermal eruptions (Scott & Cody, 2000). Rotorua township was

developed from 1890, prompting drainage of large swampy areas and lake level changes, which then triggered a phase of increased explosive activity (Scott & Cody, 2000). This stabilised till the 1930's when drilling began, with a significant increase in eruptions between the 1960's and late 1980's when many bore holes were drilled as an alternative for heating during the oil shortages of this time (Scott & Cody, 2000). During the 1970's significant geothermal surface features were disappearing, most importantly the regions geysers, which support the local economy through increased tourism. To reduce these impacts a monitoring and well closure program was established leading to reduced eruptions and slow recovery of geothermal features (Scott & Cody, 2000).

Over 91 eruptions have been recorded within the city, the most recent well known event occurring at Kuirau Park in 2001 (Doherty, 2009). Two events occurred that year, representing the first eruptions within the park since 1964. The first occurred on the 26th of January (Figure 1.6), lasting for 4 minutes, while throwing material 1200 m^3 of material 100 m into the air (Doherty, 2009; Scott et al., 2005). This threw debris across the nearby highway reaching the hospital walls (Doherty, 2009; Fullard, 2011). The second eruption occurred on the 10th of December and although longer, lasting for 1 hour, only ejected material to a height of 15 m high, leaving debris no more than 30 m from the crater (Doherty, 2009). This activity likely results from rehabilitation of the geothermal field following the well closure program in 1987. Since that time, water levels have risen between 2 and 3 m, increasing fluid pressures within the system, again priming the system for eruption (Bromley, 2003). This shows just how susceptible the natural system is to change, with both increased and decreased drilling acting to produce eruptions.

Figure 1.6: View of the eruption crater formed during the 2001 eruption at Kuirau Park (Scott et al., 2005).

1.4.7.4 *TYPE 4 - RUAPEHU*

The type 4 eruption style implies a moderate sized eruption occurring as a result of natural processes in a volcanic setting. The best New Zealand example of this is the most recent eruption from Mount Ruapehu. Since historic observations began in 1945, five of the eight major events have been predominantly phreatic in nature (Figure 1.7) (Mordret et al., 2010). The most recent of these occurred on the 25th of September 2007. This volcano is extensively monitored, with continuous data from 8 seismometers, 7 GPS stations and additional monthly gas, temperature and chemistry measurements of the lake; providing excellent information on eruptions (Doherty, 2009; Kilgour et al., 2010). At 20:16 seismic activity began, followed 10 minutes later by the eruption, lasting for only 4 minutes (Kilgour et al., 2010). This does not provide a clear enough precursor to be useful for hazard reduction (Mordret et al., 2010). It appears that the eruption was triggered when a pulse of magmatic gas from depth, caused the hydrothermal seal to rupture. The eruption formed a directed blast, covering a 40° zone towards the north, extending 2 km from the vent (Kilgour et al., 2010). This eruption also caused the crater-lake to overflow creating a surge, which almost drowned two hikers sleeping in a nearby mountain hut. One became trapped under a large boulder transported within the flow, but was rescued several hours later. Both survived and provided valuable first hand accounts of the eruption (Kilgour et al., 2010).

Figure 1.7: Phreatic eruption from Ruapehu in 1971. Image taken by P Otway (Kilgour et al., 2010).

1.4.7.5 *TYPE 5 – NGATAMARIKI*

Type 5 eruptions form medium sized events that are triggered by natural activity, occurring in a hydrothermal setting. Within the Ngatamariki region, hydrothermal eruptions are naturally occurring events. Historically two major eruptions have occurred from Orakonui South. The first and smaller event occurred in 1948 (O'Brien, 2010), while the most recent larger event occurred on the 19th of April 2005 (Milicich & Reeves, 2009; O'Brien, 2010). This larger eruption created a plume that could be seen up to 10 km away, throwing debris 100 m into the air, while falling in a 70 to 100 m radius around the crater (Milicich & Reeves, 2009). It has been estimated that between 7,000 and 10,000 m^3 of material was excavated during the 2 hour eruption (Figure 1.8), which was still producing a 10 m high steam plume 5 hours later (Milicich & Reeves, 2009). The eruption expanded the previous crater, leaving the 50 by 30 m crater seen today (O'Brien, 2010).

Figure 1.8: Orakonui South crater and debris eight days after the 2005 eruption; photo courtesy of Bruce Mountain, GNS Science.

1.4.7.6 *TYPE 6 – ROTOKAWA*

Many large historical hydrothermal eruptions have occurred at Rotokawa (Figure 1.9), reflecting the common characteristics observed in type 7 eruptions. The true number of eruptions is hard to determine from field evidence. At least 13 large events have been identified, with additional smaller events very likely (Bixley & Browne, 1988). These large events have been dated, with the most recent occurring 3,200 years ago (Collar & Browne, 1985). The earliest events are harder to date but it is likely that 7 individual eruptions occurred between 11,000 and 20,000 years ago; followed by another 3 between 9,000 and 9,700 years ago, and the more recent events occurring at 6,060 and 4,500 years ago (Bixley & Browne, 1988; Browne & Lawless, 2001). Deposits from these events cover an area of 15 km^2, with a large volume of material estimated close to 10^7 m^3, because of this excavation depths are thought to reach at least 450 m (Browne & Lawless, 2001; Collar & Browne, 1985). The initiation of these eruptions are suggested to be strongly influenced by the regional structure, with the vents following a NE trend parallel to the regional fault system (Browne & Lawless, 2001; Collar & Browne, 1985). Although the initial trigger is unknown, it is suggested that they may have been caused by lowering of the water table, which reduced the pressure allowing the liquid dominated system to flash to steam (Browne & Lawless, 2001; Collar & Browne, 1985). After the initial eruption 20,000 years ago, this may have prompted future events by creating a high permeability pathway for recharging fluids to migrate along,

thereby sending them to lower pressure areas where boiling can easily occur (Collar & Browne, 1985).

Figure 1.9: View into a hydrothermal explosion crater at Rotokawa, photo courtesy of Simon Bloomberg, University of Canterbury

1.4.7.7 *CLASSIFICATION SUMMARY*

Based on the described classification scheme and detailed examples above, a new and effective means to describe the different types of phreatic and hydrothermal eruptions is provided. This scheme allows a simple means in which to describe the eruptions based on easily observable data, without requiring extensive assumptions or interpretations. Any eruption can be classified into one of these 6 types, as long as the key information of eruption size, trigger (natural/induced), and setting (volcanic or geothermal) is known; giving the potential for this to be a universally applied classification.

Chapter Two

Experimental modelling of fragmentation processes within phreatic and hydrothermal eruptions

---

Abstract

Phreatic and hydrothermal eruptions often occur with little or no warning representing a significant hazard within geothermal regions. These violent eruptions occur at a range of temperatures and pressures within variable rock types. A range of mechanisms including heating or decompression allows hydrothermal/supercritical fluid to rapidly flash to steam, expanding and shattering the surrounding rock to produce an eruption, with no direct magmatic influence.

These eruptions are highly variable resulting in the current wide ranging classification schemes, many of which are based on characteristics that are hard to observe and define. This has resulted in confusing nomenclature with many different terms used to describe the same eruptive phenomena. Here a new classification scheme is presented, based on easily definable features of eruption size, trigger type (natural or anthropogenic) and geological setting (volcanic or hydrothermal). This ultimately produces a classification dividing the eruptions

into either phreatic, where magma interacts with cold water but no juvenile material is erupted and hydrothermal where eruption occurs from an already heated hydrothermal system.

Previous studies have focused exclusively on either physical characteristics of eruptions, small scale experimental modelling of trigger processes or mathematical modelling of various eruption characteristics. Here, a new experimental procedure has been developed to model phreatic fragmentation based on shock tube experiments for magmatic fragmentation by Alidibirov and Dingwell (1996). Water saturated samples are fragmented from a combination of argon gas overpressure and steam flashing within vesicles. These experimental results are combined with physical characteristics of density, porosity and mineralogy to develop a fragmentation model for phreatic and hydrothermal systems. This was developed with the overall aim to increase understanding of these eruptions, ultimately improving future hazard modelling.

Experiments were performed on natural explosion breccia samples (ignimbrites), collected from the Okaro explosion crater. In order to evaluate alteration effects, both unaltered ignimbrite and hydrothermally altered ignimbrite samples were analysed. Experiments were performed at room temperature and 300°C and pressures from 4 to 15 MPa, to reflect likely geothermal conditions while also assessing the effect of liquid water on fragmentation.

Results indicate that within these samples 5 to 8 MPa of decompression is required to trigger an eruption, fitting well with the previously identified trend between decompression and porosity for magmatic samples. The fragmentation front propagates through the sample at speeds ranging between 14 m/s to 42 m/s, reflecting increasing speeds with higher pressures, with no obvious impact from saturation or level of alteration. Most importantly, grain size analysis from these experiments revel a clear shift to smaller grain sizes when liquid water flashes to steam (independent of pressure or sample type), possibly reflecting greater energy involved with steam flashing.

Here, a first parameterisation of conditions for phreatic and hydrothermal eruptions is presented, along with a fragmentation model describing how these eruptions occur; illustrating stages from initial system priming and overpressure development through to the last stages of eruption and crater formation.

2.1 Introduction

Phreatic and hydrothermal eruptions are common forms of volcanism on earth, often occurring suddenly and often without warning, as with the initial phases of the 1995 Ruapehu eruption (Christenson, 2000). Although common, these systems remain poorly understood, representing a significant hazard on volcanoes and for geothermal areas. Eruption is driven by sudden decompression or heating allowing hydrothermal fluid to rapidly flash to steam, fracturing the overlying material and triggering eruption (Germanovich & Lowell, 1995). Previous studies (Browne & Lawless, 2001; Germanovich & Lowell, 1995; Hedenquist & Henley, 1985) have investigated either the physical characteristics of explosion craters or modelled eruptive processes, without the additional mechanistic benefit of experiments to link the two.

The complexity in understanding and predicting these eruptions results from the wide ranging conditions over which they occur (Browne & Lawless, 2001). Classifications have been suggested based on a wide variety of factors including fluid type, temperature, debris and eruption triggers (Smith, 2000). Many of these factors are still poorly constrained, resulting in numerous definitions for the same eruption, including phreatic and hydrothermal along with steam-blast, boiling-point or hydro-explosions (Barberi et al., 1992; Smith, 2000). Possible triggers are decompression driven e.g. landslides, dome collapse or crater-lake break-out (Browne & Lawless 2001; Spieler et al. 2004; Muffler et al. 1971), or pressurization driven from heating or volatile release by rapid magma ascent or intrusion (Nelson & Giles, 1985). In addition to natural processes, anthropogenic activity during geothermal exploration and production can also cause significant decompression, thereby triggering eruption (Hedenquist & Henley, 1985). Following the eruption trigger, porous rock fragments as water trapped in pores within the rock expands (Morgan et al., 2009). This can either produce eruptions forming from depth, shattering and lifting large amounts of material above (bottom up eruption) or eruptions initiating in the near surface propagating downwards lifting small volumes of material as it goes (top-down eruption) (Figure 1.2).

Phreatic and hydrothermal eruptions vary significantly across several orders of magnitude, and although representing highly explosive forms of volcanism, they are still significantly smaller than their magmatic counterparts (Montalto, 1995). They can last from seconds through to several hours (Buttinelli et al., 2011; Smith, 2000), creating craters varying from

just a few metres to the largest examples over 2 km in diameter (Morgan et al., 2009). As crater size varies, so does the deposit volume, ranging from a few square metres to many square kilometres, with an excellent example being the 15 km^2 prehistoric Rotokawa eruption (Collar & Browne, 1985). Extent of surface features are relatively easy to determine in contrast to the initiation depth, which must be inferred after slumping, material fall back and lake formation fills the majority of the crater (Smith & Mckibbin, 2000). Current best estimates indicate that these eruptions may excavate up to depths as great as 1.2 km (Buttinelli et al., 2011). With such variability, a new classification scheme is proposed, based on eruption size, trigger type (natural or human induced) and setting (volcanic or geothermal) (Figure 1.3), in order to better describe the kinds of eruptions.

Fragmentation can be achieved experimentally by rapid decompression, producing a pressure differential across the sample (Alidibirov & Dingwell, 1996). The minimum pressure change required to produce full fragmentation is defined as the fragmentation threshold (Spieler et al., 2004; Scheu et al., 2006). Open porosity has a significant influence, controlling the amount of gas available for decompression and therefore the energy produced during fragmentation (Spieler et al., 2004; Alatorre-Ibargüengoitia et al., 2010).

Here an experimental set-up is used, based on Alidibirov and Dingwell's (1996) shock tube experiments to produce phreatic fragmentation. Water saturated, ignimbrite samples are fragmented as a result of steam flashing within the pore spaces, due to rapid decompression at elevated temperatures (Scheu, 2012). With this set-up a wide range of conditions can be modelled, including temperature and amount of decompression. This enables direct measurement of fragmentation characteristics from grain size to velocity. All are essential parameters for understanding the processes producing phreatic and hydrothermal fragmentation. These experimental results can then be linked back to field observations to improve existing knowledge of how these eruptions occur. Our overall aim is to improve future hazard modelling to reduce the risks associated with both hydrothermal and phreatic eruptions. In order to achieve this, firstly experimental sample material from both a hydrothermal explosion breccia and its unaltered equivalent was characterised. From this the key fragmentation parameters for both sample types was determined, specifically focusing on the resultant grain size distributions before creating a model to illustrate how fragmentation occurs within phreatic and hydrothermal systems.

2.2 Sample Description

Experimental sample material was collected within the Taupo Volcanic Zone of New Zealand, from an existing explosion crater, in order to best represent natural conditions. Rangitaiki ignimbrite samples were collected from both the Okaro breccia and nearby in-situ locations giving two sample types, 1) the hydrothermally altered material and 2) the equivalent material in its unaltered form. In sample type 1) alteration is predominantly illite-smectite with 30 % illite, indicating alteration within a hydrothermal system at temperatures between 180 and 230°C (Reyes, 1990).

From both sample sets cylindrical cores were drilled, measuring 25 mm in diameter and 40 mm in length. Prior to fragmentation all cores were measured for density and porosity with helium pycnometry (Micromeritics Accupyc 1330). Type 1) altered samples have an average open porosity of 40 % and type 2 unaltered samples have an average open porosity of 24 %, both with closed porosities less than 1 %. Porosity differs as a result of silica removal associated with alteration of primary mineral phases, causing a net change in rock density (Pochee, 2010). Full details of sample preparation are given in Appendix A.

2.3 Experimental Methods

Several studies have been completed using the fragmentation device of Alidibirov and Dingwell (1996) to investigate magmatic fragmentation, with only preliminary experiments investigating phreatic fragmentation (Scheu & Dingwell, 2010; Serr, 2010). The fragmentation "bomb" is a shock tube apparatus made up of three main components (Figure 2.1). Firstly a high pressure autoclave containing the sample is used to represent the conduit. Above which is a large tank (3 m high and 0.4 m in diameter) at atmospheric pressure where the fragmented material is caught. These two components are separated by a set of scored diaphragms, allowing opening of the pressurised autoclave at precisely calibrated pressures (e.g. Alidibirov & Dingwell 1996; Spieler et al., 2004; Alatorre-Ibargüengoitia et al., 2010). Using samples saturated with liquid water, this set-up can be used to investigate phreatic and hydrothermal fragmentation (Appendix A).

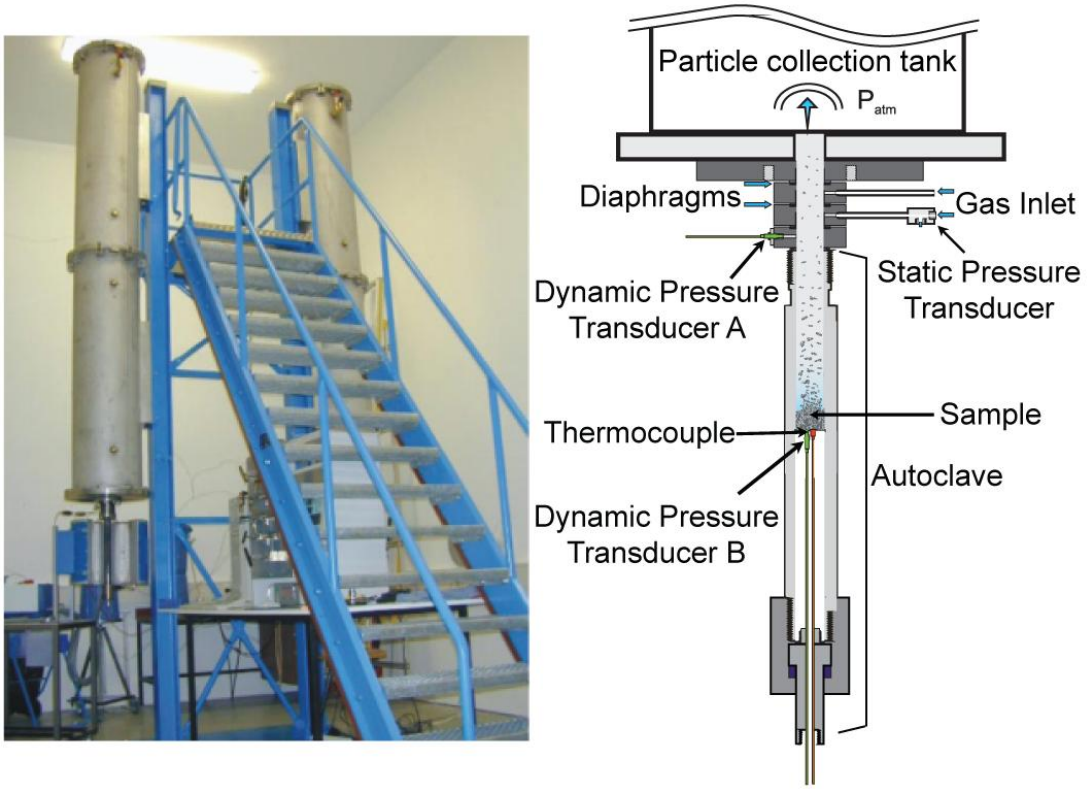

Figure 2.1: Experimental set-up of the fragmentation bomb (left) and details of the phreatic autoclave (right). The photo shows two fragmentation bombs, with large tanks where particles are collected sitting above the furnace and autoclave. The schematic autoclave shows the sample location in respect to the pressure transducers, thermocouple and diaphragms.

To trigger fragmentation, overpressure is used to induce failure of the diaphragms, with the upper diaphragm bursting first, followed almost simultaneously by the lower (Spieler et al., 2004). Rapid decompression of the autoclave occurs, producing a pressure gradient with the sample. Liquid water and/or gas within the pore spaces of the sample will expand, and if the pressure gradient is high enough, will fragment the sample. If not, permeable degassing will occur (Spieler et al., 2003; Spieler et al., 2004; Mueller et al., 2008).

A variety of fragmentation experiments were performed to investigate the effects of saturation, alteration and temperature. To obtain initial baseline data, dry argon gas experiments were performed on both altered and unaltered ignimbrite, then as a comparison the same experiments were completed with liquid water saturated samples. Both argon and liquid water experiments were run at a variety of pressures (ranging from 4 MPa through to 15 MPa) and two temperature conditions (room temperature and 300°C). These temperatures were chosen to separate the effect of water weakening (Vásárhelyi & Ván, 2006), from that of

steam flashing in a typical hydrothermal system. This temperature (300°C) was considered typical of conditions immediately prior to fragmentation in a hydrothermal system as a result of sudden heat flux (for instance from a dyke intrusion), rapidly increasing temperatures prior to fragmentation, without necessarily affecting the temperature recorded in the alteration assemblage.

Fragmentation velocities were obtained by measuring the time the fragmentation front takes to travel through the sample. Dynamic pressure sensors placed above and below the sample record when the pressure drops thereby indicating the start and end of the sample's fragmentation (Scheu et al., 2006). Using fragmentation time and sample length, the velocity of the fragmentation front can be easily calculated.

After fragmentation, particles are caught in the large upper tank. Rinsing this tank with pressurised (8.5 MPa) desalinated water, enables recovery of more than 99% of particles (Kueppers et al., 2006). The particles are washed from the tank through a 125 μm sieve, separating out a coarse and fine fraction. The coarse fraction is dry sieved at half-Φ intervals down to 3.5 Φ, while the fines are analysed using a Beckman-Coulter LS230 for laser refraction (Kueppers, 2005).

2.4 Results

2.4.1 Fragmentation Thresholds

A fragmentation threshold is the minimum pressure change required to produce full fragmentation (Spieler, et al., 2004). This is strongly dependent on the open porosity, displaying an inversely proportional trend, with higher porosity samples fragmenting at much lower pressure differentials than those with lower porosities (Spieler et al., 2004; Kennedy et al., 2005; Scheu et al., 2006; Mueller et al., 2008). Temperature appears to have only a minor influence, with previous work indicating that increasing temperature lowers the fragmentation threshold for samples with porosities in a similar range to those tested here (Kueppers, 2005). This threshold reduction, falls within the range of values obtained here so this is considered to be within the error and of little influence. These trends were previously identified through

experiments performed on primary volcanic rocks. Here the results of some of the first experiments on clastic rocks are described (raw data is presented in Appendix B).

Initial experiments were completed to obtain dry fragmentation thresholds for both altered and unaltered material. Results compare well with those of previous experiments (Figure 2.2). The inversely proportional relationship between porosity and threshold holds, however there is some variation, with results ranging between 5 and 8 MPa and no clear trend as a result of temperature changes.

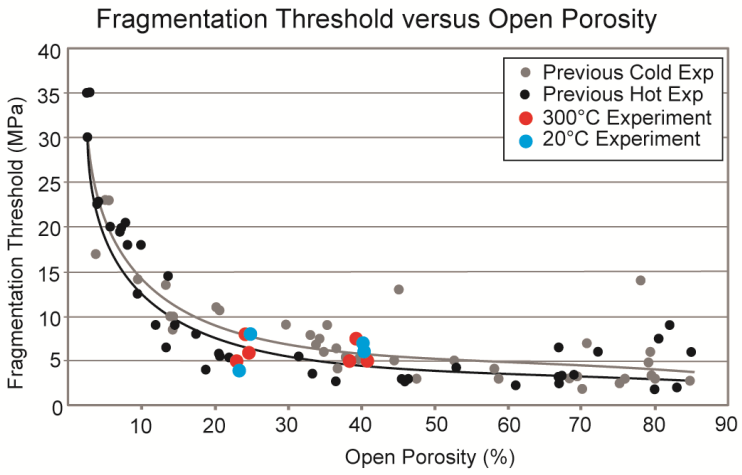

Figure 2.2: New fragmentation thresholds for ignimbrites plotted with data from previous experiments on volcanic samples. A clear correlation exists, indicating that the previously identified inversely proportional relationship between threshold and porosity holds (Spieler et al., 2004).

2.4.2 FRAGMENTATION SPEED

After fragmentation thresholds had been established, experiments were performed just above the threshold at 8 and 10 MPa, then significantly above the threshold at 15 MPa. These pressures ensured full fragmentation, and provided accurate pressure recordings essential for speed analysis. Speeds range from 14 to 42 m/s, showing a wide scatter but with key trends still apparent (Figure 2.3).

Variability within these results is probably caused through natural variation of the samples themselves. Previous experiments performed on primary volcanic rocks, show much clearer trends resulting from the more homogenous nature of the sample material. Trends shown

within these results suggest that overall higher applied pressures produce faster fragmentation speeds. Within the different sample types, altered samples appear to fragment faster than their unaltered equivalent. This is likely due to their higher porosities and therefore greater potential energy. Interestingly, experiment type (argon gas or liquid water) does not appear to influence the speed. All fragmentation speeds were measured from experiments performed at 300°C, so no comment can be made on the influence of temperature.

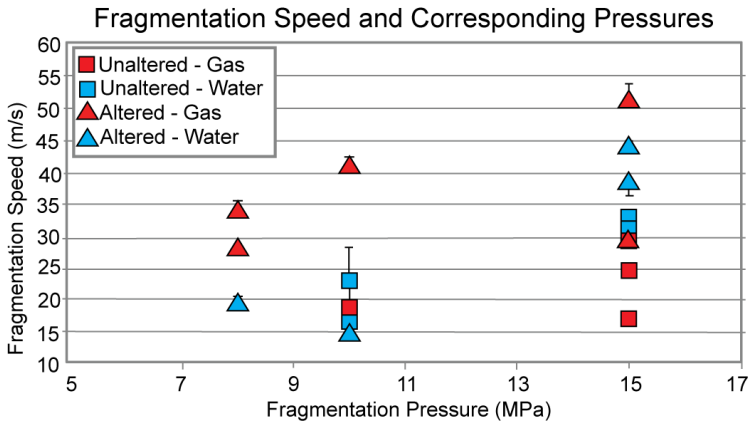

Figure 2.3: Fragmentation pressure and resultant speeds from experiments performed at 300°C. Although showing significant scatter, this illustrates the key trends of increasing speed with higher pressure, alteration or porosity. Note that error bars exist for all points, some are just too small to be visible at this scale.

2.4.3 Grain Size Analysis

After determining fragmentation speed, grain size analysis was completed. Samples that were water saturated prior to decompression showed a smaller grain size compared to those that were saturated in argon gas and decompressed. Additional smaller affects were indicated by alteration and porosity. Experiments were repeated to determine the accuracy of grain size distributions, with results showing almost identical weight fractions at each size interval, confirming reproducibility. As with the fragmentation speed analysis, only experiments performed at 300°C were analysed here.

Directly comparing argon gas experiments with liquid water experiments shows the influence that steam flashing has on grain size (Figure 2.4, c). With liquid water experiments, grain sizes are significantly reduced and develop a greater distribution in comparison to the sharp

peak of predominant grain sizes within the argon gas experiments (Figure 2.4, a and b). In contrast to the influence of liquid water, there is only minor change as a result of either pressure or sample alteration and differing porosities (Figure 2.4, a and b). Increasing pressure and/or level of alteration seems to produce slightly smaller grain sizes, as seen within both water saturated and argon gas experiments. However this trend is more pronounced for the water saturated samples.

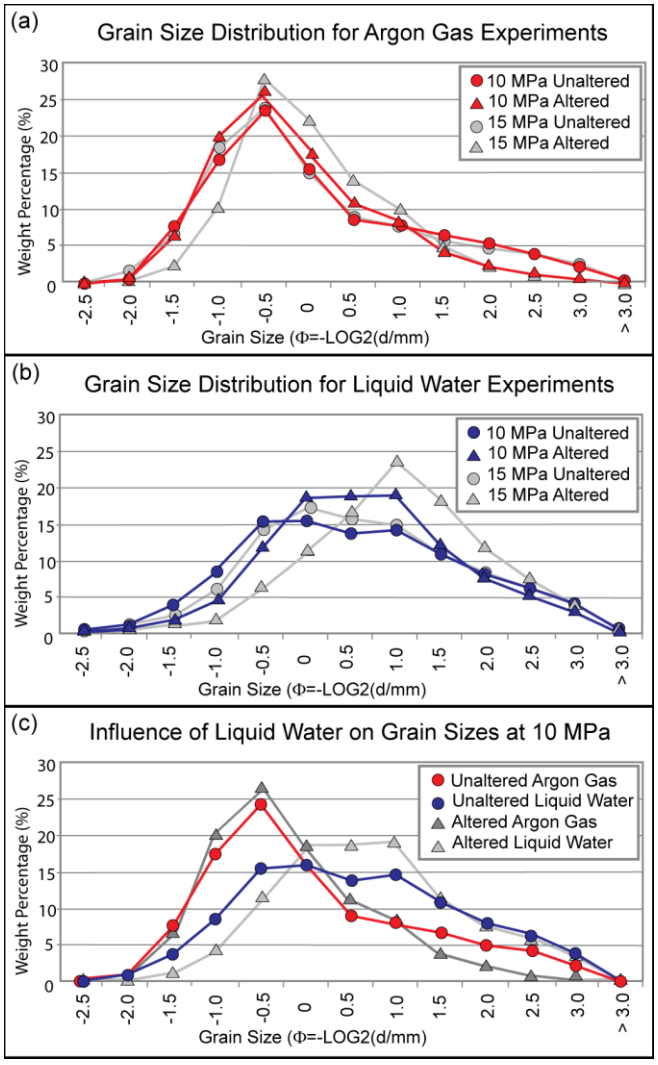

Figure 2.4: Grain size distributions for argon gas (a) and liquid water (b) experiments run on both sample types at 10MPa and 15MPa; with a comparison of grain size distributions between both experiments run at 10 MPa (c), to illustrate the influence of saturation. The argon gas experiments show coarser grain sizes while the liquid water experiments show finer grain sizes over a greater range. Note that all results here reflect experiments performed at 300 °C, therefore no comments can be made about influence of temperature on grain size.

2.4.4 Fragmentation Energy

Fragmentation energy was calculated to determine how increasing energy influences grain sizes and fragmentation speed. This energy relates to the amount of expansion that occurs on decompression. For the argon gas experiments, where there is only gas expansion, the level of energy released is generally lower than that of the liquid water experiments where predominantly steam flashing occurs. Fragmentation energy is calculated as the energy produced by both liquid and gas expansion in relation to the calculated volume of the sample (Mastin, 1995; Scheu et al., 2012; Thiéry & Mercury, 2009). The energy is then normalised to a unit volume, allowing a comparison between the results of this study and that of previous ones with varying sample sizes. To calculate the specific energy released from argon gas expansion Ea (in J/cm^3), the experimental pressure P (in MPa), is multiplied by the normalised gas volume V of a sample, α gas, as in the following equation:

$$Ea = P\ x\ \alpha\ gas$$

To then calculate the energy Ew, released by the flashing of liquid water to steam (in J/cm^3), an approximation of 50 J/g is used, based on Thiery and Mercury's (2009) suggested expansion work for irreversible adiabatic expansion around 300°C. To calculate this value is simply multiplied by the amount of water added m (g), as follows:

$$Ew = 50\ x\ m$$

In order to directly compare Ea and Ew, Ew needs also to be normalized to a unit volume. The detailed conversion is given at Scheu et al. (2012). For this study, this results in exactly the same values as calculated for Ew, but with the unit of (J/cm^3). Combining these two values gives the total energy for fragmentation from both steam flashing and argon gas expansion. Comparing the energy produced to the mean grain size, shows that with higher energy the resultant grain sizes are reduced (Figure 2.5).

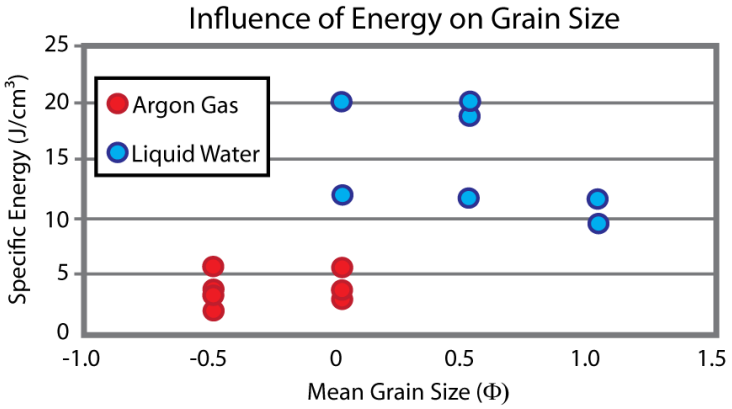

Figure 2.5: Mean grain size versus energy released for both argon gas and liquid water experiments.

2.4.5 KEY RESULTS

The key results can be summarised as follows:

1) Fragmentation thresholds for both unaltered and altered ignimbrites fit well within the trend of previously published results.
2) Fragmentation speed ranges between 14 and 42 m/s.
3) Grain sizes are greatly reduced with saturation, independent of sample type or pressure.
4) Fragmentation energy increases with saturation.
5) Higher fragmentation energy results in smaller grain sizes.

2.5 SOURCES OF ERROR

Within the experimental methods used here, there are several sources of error, all of which contribute a certain level of variability to these results. Error can be introduced through all stages of analysis while determining the fragmentation threshold, speed, grain size and energy. Below the different sources of error are discussed and where possible their magnitudes are defined. Even though samples were drilled from the same rock, there is a certain amount of sample variability that can account for the small discrepancies between repeated experiments under the same conditions.

The accuracy of fragmentation thresholds is limited by the tested pressure intervals. To determine fragmentation thresholds, the pressure is increased in 1 MPa intervals. This means that the thresholds are accurate to the nearest whole MPa. This takes into account any variability within the diaphragms, which is checked through repeat experiments.

Within the speed data, error bars (Figure 2.3) illustrate the variability introduced by human interpretation. When calculating fragmentation speed, the point at which the pressure drops is hand picked from pressure curves. The error bars illustrate the first and last possible points at which this could occur, thereby corresponding to the slowest and fastest possible speeds. These calculated errors reach a maximum of 5.4 m/s, with an overall median error of only 1.5 m/s. Repeat experiments show significant variation from 0.4 m/s difference between repeats, through to a 20 m/s difference, with a mean variation of 7 m/s. This occurs over all experiment types and pressure ranges, suggesting that there is simply significant variation in speed.

Grain size reproducibility is checked by running repeat experiments. These show agreeable results in most instances, with only three exceptions of significant variation, caused through sample loss during collection. A maximum variability of 8.8 g was observed for only one experiment, with a much lower average of 1.3 g variation. Additional variability can be introduced through error within the electronic scales and losses during the sieving process itself.

Within the energy calculations, error is largely introduced through determination of porosity and saturation. When measuring porosity, error is introduced through irregularities in the sample length and diameter which vary up to 0.5 mm and 3 mm respectively. This introduces error in the geometric volume of the sample and therefore the final porosity. Before running the pycnometer, oven dried samples must be weighed. This introduces error as the samples immediately start absorbing water on leaving the oven, slightly adding to the weight. Electronic scales measure to 4 decimal places, thereby adding only minimal error. Measurements performed within the pycnometer have very low variability with standard deviations on volume measurements lower than 0.02 cm^3 and less than 0.005 g/cm^3 for density. When determining saturation, error can again be introduced when weighing the oven dried samples, as discussed above, with the most significant error arising while measuring the water saturated samples. After removing from a water bath under vacuum, the sample is

surface dried to remove additional water before weighing. Variability is introduced depending on how much water is removed. These two parameters – porosity and percentage of liquid water saturation, are the key to energy determination. Additional variability may be introduced simply through human error and loss of accuracy during calculations (for instance removing decimal places). Results suggest this error can be up to 10%.

2.6 Discussion

The above findings derive from a series of rapid fragmentation experiments on natural samples collected to model the way in which phreatic and hydrothermal explosions occur. As these eruptions occur rapidly with little warning, there are very few detailed observations or measurements that can be applied to understanding the fragmentation process. In most instances, information obtained from these explosions comes from deposits studied well after the eruptions have ceased. Here experimental procedures were used to obtain an insight into these processes, gaining information that observations alone can not provide.

Although phreatic and hydrothermal explosions can occur at varying scales from meters to kilometres (Morgan et al., 2009), the experimental results discussed here are applied to a medium sized eruption. For example, the type 5 Lake Okaro or Ngatamariki described in Figure 1.3. Experimental fragmentation thresholds obtained with argon gas, suggest that fragmentation could be initiated with 5 to 8 MPa of decompression, if initiating within ignimbrite (or rock of similar properties) from a hydrothermal system in either a liquid or gaseous phase. Despite being the first experiments performed on natural ignimbrites, these thresholds match that of the earlier results from lava flow rocks. Additionally, there is no significant difference between fragmentation thresholds obtained at high temperatures versus those at lower temperatures, consistent with the findings by Keuppers (2005). These findings suggest that neither sample material nor temperature has a significant influence on the fragmentation threshold and that porosity remains the dominant factor. Therefore where a hydrothermal system exists and the porosity of the overlying material is known, the decompression required to trigger eruption can be estimated with the established threshold and porosity relationship.

Results of fragmentation speed analysis show two key trends. This suggests that both higher applied pressures and alteration (corresponding to higher porosities) produce faster fragmentation speeds (Figure 2.3). Results indicate that fragmentation occurs at a speed between 14 and 42 m/s. Overall these speeds are slightly lower than that obtained in the initial phreatic fragmentation study performed by Serr (2010); where sandstones with an average 27% porosity were fragmented at speeds ranging between 39 and 60 m/s. These lower speeds may be caused through the slightly lower porosities. Previous work (Scheu et al., 2006) suggests that speed is highly influenced by porosity and shows that samples between 20 and 33 % porosity (similar to those within this study) should exhibit speeds between 20 and 40 m/s when fragmented at 10 to 15 MPa. Also shown in the Scheu et al. (2006) study is the influence of pressure, where higher pressure differentials result in faster fragmentation speeds. These findings are consistent with the speeds obtained here. Results from both Serr (2010) and Spieler et al. (2004) suggest that there is no difference between speeds at higher temperatures (up to 950°C) and that of cooler temperatures (20°C), as is also apparent within our results.

Grain size analysis after fragmentation provides a measure of the influence liquid water has on fragmentation efficiency. It is assumed that in natural eruptions there is a reduction in grain sizes as a result of flashing (Wohletz 1983; Cronin et al., 2003). Our experimental results prove a clear relationship showing that the average grain size is reduced when starting conditions involve liquid water, in comparison to those performed with argon gas (Figure 2.4, part c). This explains why smaller grain sizes are produced from liquid dominated hydrothermal systems in comparison to vapour dominated systems. When compared to results from previous experiments (Scheu & Dingwell, 2010) performed on samples with similar porosity, at pressures and temperatures similar to those used here, the same trend is observed. This suggests that grain size reduction occurs independently from alteration intensity, as the previous experiments were performed on fresh unaltered material, at very similar pressures while producing the same effect. Previous work by Kueppers et al. (2006) identified a key trend showing that smaller grain sizes are produced with greater fragmentation energy, resulting from either higher applied pressures or higher porosities. Within the range of porosities (24 to 40%) and pressures (up to 15 MPa) used for our experiments these effects are also shown although somewhat masked by sample variability (Figure 2.4).

Grain size distributions from experimentally generated pyroclasts, are comparable with natural deposits because grain sizes are dependent on fragmentation mechanisms occurring at less than mm scales, no matter if naturally or experimentally derived (Wohletz, 1983). Comparison between the experimentally derived fragments in this study and grain size analysis of the Okaro eruption breccia (from where our sample material was collected) performed by Hardy (2005) show a similar range of sizes. Hardy (2005) shows the highest weight percentage of fragments in the 0 to 1.5 phi range, with some as large as -1.5 phi and outliers of -3.5 phi. Our experimentally derived particles fit right within this range, with the highest weight percentage of particles in the range of -0.5 to 1.0 phi.

Reduced grain sizes seen in experiments performed with liquid water can be explained by the increased energy production associated with these explosions (Wohletz, 1983). Fragmentation is driven by expansion of vapour trapped within confined pore spaces and fracture networks of rocks. Where the starting conditions are gas, only gas expansion will occur. When the starting conditions are a liquid, steam flashing occurs, resulting in much a much greater volume change than that of pure gas expansion. With greater volume change, more energy is produced resulting in improved fragmentation efficiency. In addition to greater energy with steam flashing, water can act to weaken the rock strength and further reduce particle sizes (Baud & Zhu, 2000; Vásárhelyi & Ván, 2006). Future studies should investigate this effect in conjunction with fragmentation.

The following model (Figure 2.6) combines experimental fragmentation results with field interpretations and previous case studies (Figure 1.3). A simple hydrothermal system exists, either as a liquid or vapour dominated system, which can be primed for eruption if pressure and/or temperature increases at a rate faster than it can be released by permeable flow. This can occur due to the formation of a cap rock and reduction in permeability or solely with increased pressure or temperature flux (Figure 2.6, a). When primed, a trigger acts to initiate the release of overpressure, creating a fracture pathway from the hydrothermal system to atmospheric conditions (Figure 2.6, b). Although trigger mechanisms vary widely the most commonly suggested is seismic activity (Browne & Lawless, 2001). Self rupture can also occur if overpressure becomes too high, as in hydrofracturing (Cobbing & Dochartaigh,

2007). With a decompression pathway created, fragmentation can begin propagating out from the fracture surface. Continued expansion of fluid in pores within the hydrothermal system causes ejection of blocks of overlying material, creating a crater and allowing the fragmenting material to be ejected (Figure 2.6, c). With continued fragmentation and material ejection the crater develops, with sides slumping and material falling back into the crater. Some clasts may be repeatedly erupted as fragmentation proceeds laterally and vertically downwards, into the over-pressurised saturated porous rock. After excavation to maximum depth, eruption may continue for some time with a more geyser like style (Figure 2.6, d). As the fragmentation front excavates rapidly, likely between 14 and 42 m/s as suggested by these experiments, in order to reach a depth of 100 m it would take a maximum of 7 s. Observations of historic events have indicated eruptions last much longer, for instance the 2005 Ngatamariki eruption which lasted for two hours, with steam still being produced five hours later (Milicich & Reeves, 2009). For eruptions of these lengths, geyser style activity must occur after the flashing front has finished propagating in order to produce such long running events; this is likely to continue until the hydrothermal system becomes depleted and no further flashing can occur. Future studies should test a wider range of lithologies, to further validate this model, making it more applicable to a wider range of eruptions.

2.7 Conclusion

Here experimental fragmentation techniques first described by Alidibirov and Dingwell (1996) were applied to phreatic and hydrothermal explosions along with data from field observations and previous literature, in order to build a model. With this method, has been shown that the pressures required to initiate these eruptions are similar to those required for magmatic eruptions. It was also determined how steam flashing acts to increase the fragmentation efficiency and reduce grain size as a result of the increased energy associated with liquid flashing to gas. This allows a proposed model of fragmentation initiation to be produced. Improved understanding of the processes that produce these eruptions is essential to predict where and when they may occur, in order to reduce the risk and hazards associated with these currently unpredictable eruptions.

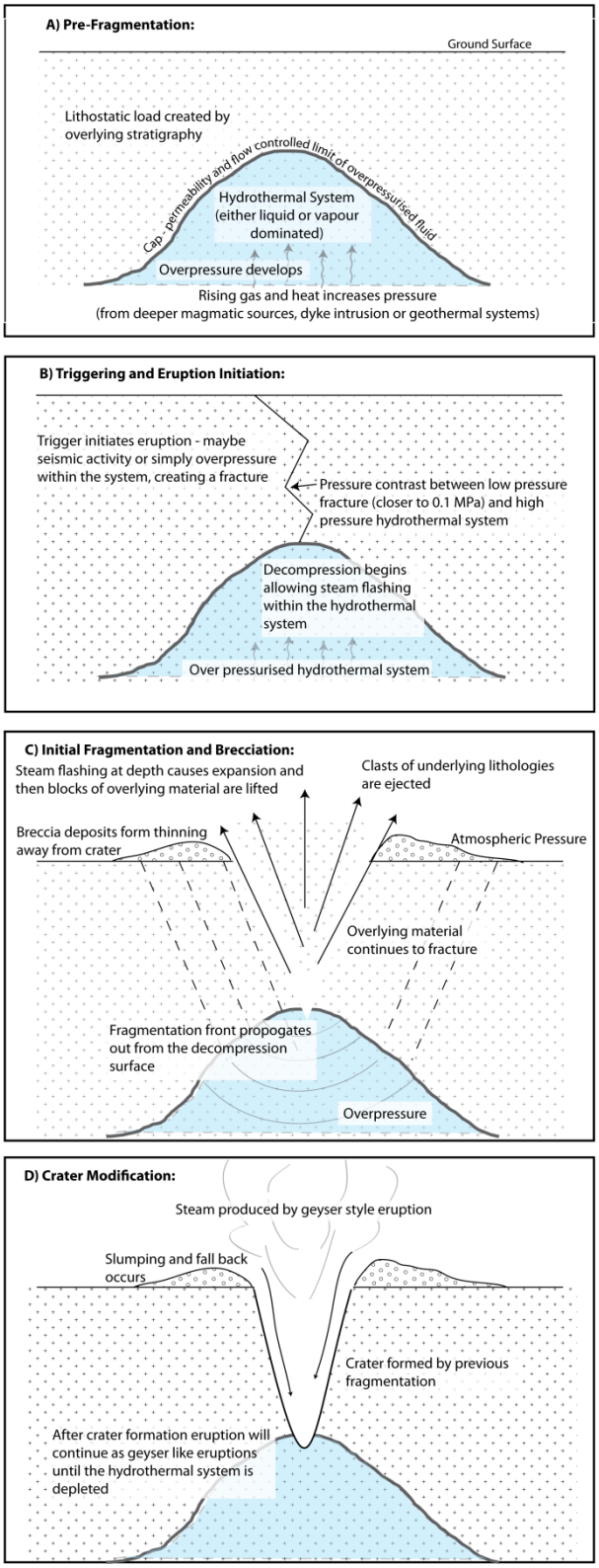

Figure 2.6: Schematic model illustrating a possible sequence of events leading to eruption initiation and crater formation. a) the hydrothermal system prior to fragmentation, b) triggering and initiation, c) initial fragmentation and brecciation, d) crater excavation.

Chapter Three

Experimental modelling of the eruption forming Lake Okaro

3.1 Introduction

While the previous discussion focused on generalised fragmentation within phreatic and hydrothermal eruptions; here the same processes will be applied specifically to model the eruption forming Lake Okaro. The study of specific eruptions, such as Okaro, is an essential step in improving current understanding of how these eruptions operate. With improved knowledge of individual eruptions, eventually a better understanding of all eruption processes can be established, with the ultimate goal to prevent hazards associated with future eruptions.

Here the methods and results from both field and experimental studies will be used to ultimately create an eruption model describing how the eruption at Lake Okaro occurred. Very few geological studies have focused specifically on Lake Okaro, with the exception of Hardy (2005), who created an eruption model based upon field observations. Here this model is built upon with the addition of recent field data and experimental results. This included data that was not discussed in Chapter 3, as it contains significant error but can still help improve our understanding of the Okaro eruption.

3.2 STUDY AREA: LAKE OKARO, TAUPO VOLCANIC ZONE

3.2.1 GEOLOGICAL SETTING

Lake Okaro is an explosion crater formed through phreatic and hydrothermal eruptions 700 years ago (Hardy, 2005). It represents a type 3 eruption style (as discussed in Chapter 1), meaning that a medium sized eruption occurred within a geothermal setting as a result of natural triggers. Located within the central Taupo Volcanic Zone (TVZ), the lake is situated 20 km south-east of Rotorua City, 10 km south-west of Mount Tarawera and forms part of the Waiotapu geothermal system. Many explosion craters occur within this region, related to the nearby Ngapouri fault (Figure 3.1), with many located on or within 1.5 km of the fault trace (Hedenquist & Henley 1985; Nairn et al., 2004). A high conductivity zone is present within this area suggesting that the Ngapouri fault forms a zone of major geothermal up-flow, most likely providing the eruptions with a fluid source (Nairn et al., 2004).

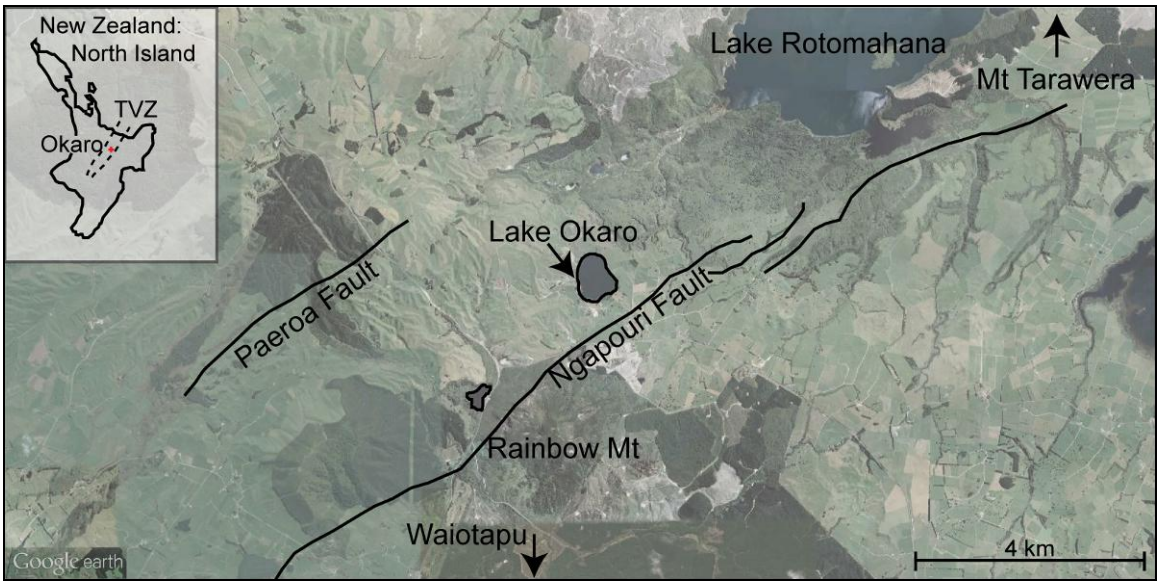

Figure 3.1: Aerial photo showing key geological features within the Okaro region (After Hardy, 2005; Hedenquist & Henley, 1985; Institute of Geological and Nuclear Sciences, 2004).

3.2.2 ERUPTIVE HISTORY OF LAKE OKARO

The Lake Okaro eruption is closely linked with the Kaharoa eruption phase from Mount Tarawera volcano (Nairn et al., 2004). Both the Tarawera and Okaro eruptions are thought to be primed for eruption by intrusion of a series of basaltic dykes. These dykes intruded the

Kaharoa rhyolite between 5 and 7 km depth (as indicated by basaltic inclusions) and are thought to have triggered the Tarawera eruption. From this it is inferred that the Okaro eruption was most likely primed by a dyke that did not reach the Rhyolite, maybe causing initial fracturing but most importantly proving additional gas and heat to the system. Additional evidence is provided by alteration suggesting a significant CO_2 flux, most likely coming from these basaltic dykes (Nairn et al., 2004). With the system primed, only a small trigger was required to initiate the eruption (Browne & Lawless, 2001).

3.2.3 CRATER MORPHOLOGY

Today the crater-lake forms a roughly oval shape, with a maximum 700 m diameter covering a 3 ha area (Cronin et al., 2006; Google Inc 2011). Post eruption slumping and fall back during eruption filled most of the crater with debris. As a result the average lake depth is 15 m, reaching a maximum 18 m in the south-western corner (Irwin, 1974), which may represent remnants of the main vent location. Hedenquist and Henley (1985) estimated that the vent excavated to 100 m depth; based on an eruption breccia volume of $3.7x10^6$ m^3 (Cross, 1963), with an average 2.0 g/cm^3 density and a crater shape between an inverted cone and cylinder.

Surrounding the crater are thick breccia deposits, with the largest volumes observed near the south-western corner measuring up to 12 m thick. This location is consistent with the deepest part of the lake, providing additional evidence to suggest that this was once the main vent. Breccia deposits thin rapidly away from the lake, with the last deposits observed 1300 m from the shoreline (Cross, 1963).

3.2.4 SUBSURFACE LITHOLOGY

Clasts found within hydrothermal and phreatic eruption breccias reflect the underlying lithologies and can provide valuable information to reconstruct how these eruptions occurred, most importantly the initiation depth. With no accurate stratigraphic record from bore holes at Lake Okaro, the main units have been determined from a variety of sources including field observations, airfall maps, nearby bore logs and early reports to create a composite stratigraphic log (Hardy, 2005; Hedenquist & Henley, 1985; Molloy et al., 2008; Nairn, 1984; Speed et al., 2002; Wilson & Walker, 1985). Assuming an original crater excavation depth of

100 m (Hedenquist & Henley, 1985), this suggests the eruption excavated several airfall units, the much thicker Earthquake Flat pyroclastics, Rotoiti pyroclastics, Rangitaiki ignimbrite and finally a siltstone layer (Figure 3.2). These units have all been observed within the Okaro breccia deposits during field sampling.

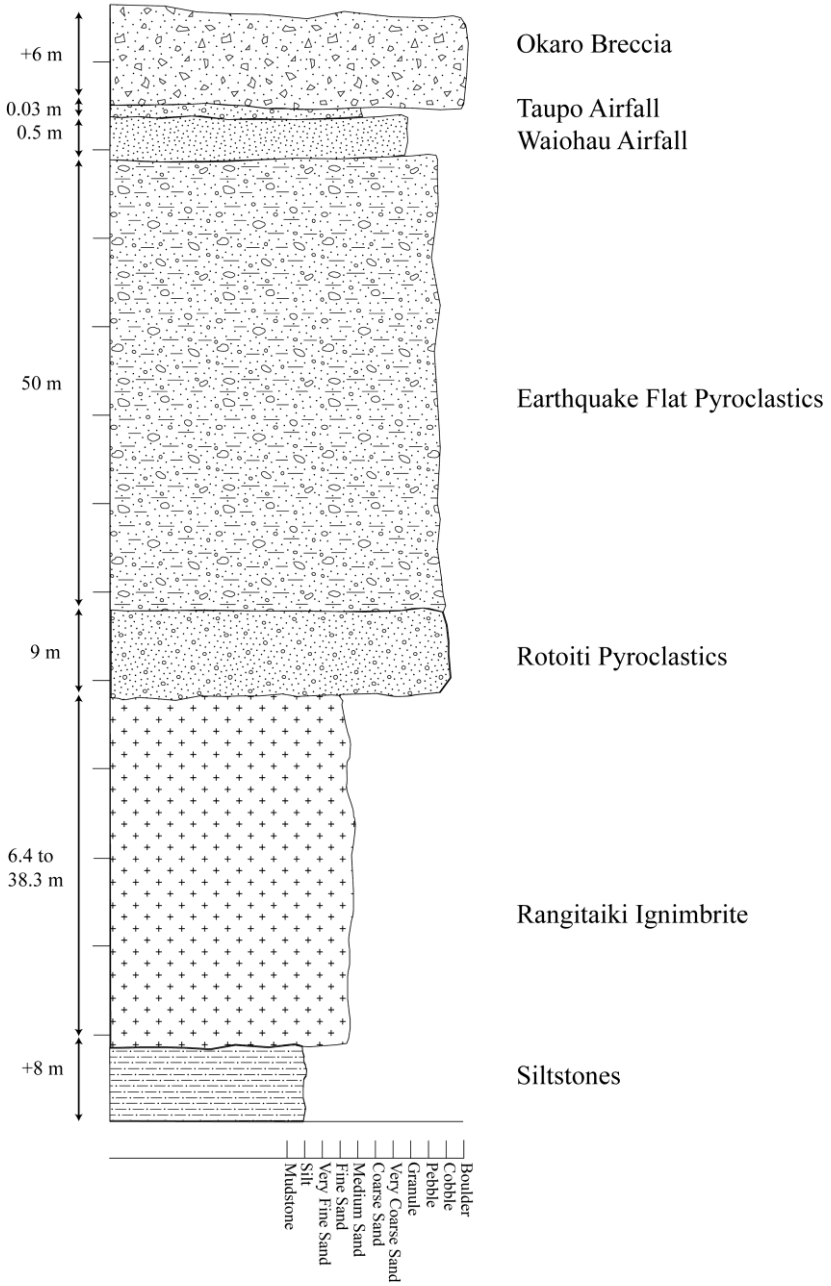

Figure 3.2: Schematic cross section illustrating the major units likely to be erupted at Okaro (Based on data from Hardy, 2005; Hedenquist & Henley, 1985; Molloy et al., 2008; Nairn, 1984; Speed et al., 2002; Walker & Wilson, 1983)

3.2.5 REGIONAL HYDROLOGY

Various drill holes and bore logs surrounding Lake Okaro have intersected water, at some sites boiling water, suggesting that the hydrothermal system beneath the lake is still active. In a study by MacFarlan (1990), hand auger holes identified a range of hydrothermal features at sites around the lake. Approximately 600 m east of the lake, three holes show boiling or superheated steam at a depths less than 5 m (Site F, Figure 3.3), while less than 100 m further east cold water was observed (Site G, Figure 3.3). Other sites around the lake intersected cold or no groundwater (Sites A, B, C and E; Figure 3.3). An additional well drilled by Environment Bay of Plenty south of the lake, encountered "warm" water at approximately 40 m depth (Site D, Figure 3.3) (Hardy, 2005; Nairn, 2003). These changes around the lake suggest significant variability within the shallow geothermal system.

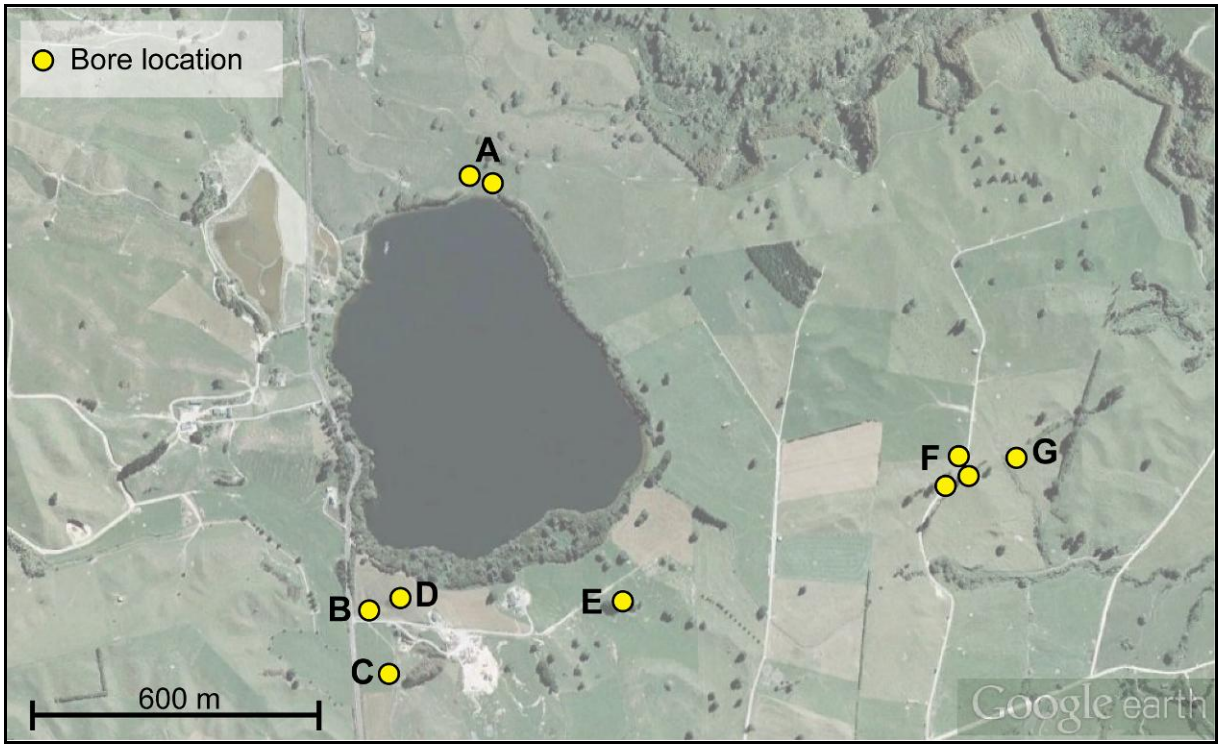

Figure 3.3: Locations of bore holes previously drilled around Lake Okaro (Hardy, 2005; MacFarlan, 1990; Nairn, 1984)

3.3 METHODOLOGY

Key methods involved with the preparation, running and processing of fragmentation experiments have been discussed in Chapters 1 and 2. Here additional methodology required to apply these result to the Lake Okaro case study will be discussed.

3.3.1 FIELD SAMPLING

Detailed field investigations, during February 2011, involved visiting and logging all breccia exposed around the lake, including any outcrops exposed within nearby farmland. Large ballistic samples were collected from any suitable outcrops.

Field analysis of eruption breccia provides an indication of lithologies that the eruption excavated through. Based on stratigraphic reconstruction there are several minor units along with two much thicker deposits, the Earthquake Flat Pyroclastics and the Rangitaiki ignimbrite (Figure 3.2). The stratigraphically deepest unit observed within the breccia is a finely laminated siltstone (Figure 3.4), occurring stratigraphically beneath the Rangitaiki ignimbrite. Despite being the deepest unit, this siltstone only represents a small proportion of clasts observed within the breccia (less than 1%). With so few clasts, this would not provide enough material to perform the fragmentation experiments; instead these experiments were run with the Rangitaiki ignimbrite.

There are several advantages for using the Rangitaiki ignimbrite as the focus of this experimental work. It makes up a high proportion of clasts, representing 20 to 40% of the breccia (Hardy, 2005). It is the only welded unit within this stratigraphy and therefore is the strongest, forming the ideal sample material because measured fragmentation parameters will suggest an upper limit for this eruption. Additionally, all Rangitaiki clasts within the breccia display alteration, suggesting that prior to eruption the hydrothermal system extended throughout this unit. In several locations small chunks of silicified material were found within the breccia. This suggests that a silica seal developed on the hydrothermal system acting as a caprock.

Figure 3.4: Clasts of finely laminated siltstone (scraped area) exposed within the Okaro breccia deposit (note scale, pen measures 14 cm in length).

To evaluate the effects that alteration has on fragmentation processes, unaltered in-situ samples were also collected, representing breccia clasts prior to hydrothermal alteration. Altered breccia clasts were collected from farmland east of the lake (S 38°18'08.1", E176°23'58.0"), while the unaltered material was collected from the Okataina caldera wall 9 km from the lake (S 38°16'35.9", E 176°29'38.9").

3.3.2 DETERMINATION OF EXPERIMENTAL PARAMETERS

Prior to the experimental phase, key parameters were determined to best represent the conditions occurring during the eruption at Okaro as well as enabling achievable experimental conditions.

3.3.2.1 *EXPERIMENTAL TEMPERATURE*

Alteration observed within the breccia can provide an indication of the temperatures found within the hydrothermal system prior to fragmentation. Rangitaiki ignimbrite clasts found within the breccia show predominantly illite-smectite alteration, with 30% illite, indicating formation temperatures between 120° and 170°C (Srodon & Eberl, 1984). These reflect realistic equilibrium temperatures within the geothermal system as it is uncommon to find

temperatures over 200°C at such shallow depths, unless the system is highly enriched in dissolved salts (White et al., 1971). However the current model for the Okaro eruption suggests that it is primed by dyke intrusion, which would have provided a sudden heat flux to the system, occurring too fast to be recorded within the alteration assemblage. For this reason, a temperature of ~250-350°C was more likely, therefore an experimental temperature of 300°C was chosen.

One disadvantage of using higher experimental temperatures, is that in order to ensure the water stays in the liquid phase until fragmentation, the corresponding pressures are limited within the lower end of the scale, where this experimental work is focused. For these liquid water experiments, the pressure and temperature conditions must be carefully monitored to ensure the fluid remains as a liquid until triggering. When using an experimental temperature of 300°C, in order to ensure that the water stays in a liquid phase the corresponding pressure must be greater than 8.5 MPa (Figure 3.5). Here 10 MPa was used as the minimum pressure (within the liquid water experiments) to ensure that it stays well above the phase transition (Figure 3.5). If experiments were performed at a lower temperature, lower pressures could also be tested. For example if the experiments were run at 150°C, pressures as low as 1 MPa could easily be used.

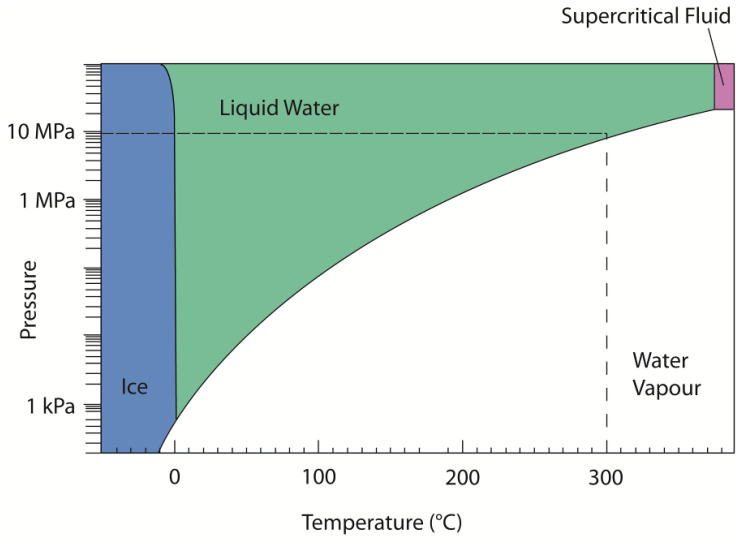

Figure 3.5: Phase diagram of water illustrating the pressure and temperature conditions required to ensure that the water stays in a liquid phase prior to triggering. This diagram illustrates one of the experiment types run at 300°C and 10 MPa.

3.3.2.2 *Experimental Pressure*

As a first step, fragmentation threshold experiments were performed, to provide a guideline for pressures required within the remaining experiments. The threshold experiments provide minimum pressures at which fragmentation will occur, while additional experiments were run at higher pressures ensuring full fragmentation every time and accurate measurement of fragmentation parameters. Unaltered Rangitaiki ignimbrite fragmentation thresholds range between 4 and 8 MPa, while the unaltered samples fragment between 5 and 7.5 MPa. Based on these values, further experiments were run on both sample types at 10 and 15 MPa, Additional comparison experiments were performed on the altered material at 8 MPa, providing extra fragmentation speed data.

3.3.3 Particle Analysis

High speed video analysis of fragmentation experiments, enable an estimation of the particle ejection speeds that are likely to be observed after fragmentation. This also enables an experimental check on ballistic speeds. Representative experiments were performed at 15 MPa and captured on high speed video recording of 15,000 frames per second. This footage was then analysed using ImageJ software, with the MTrackJ particle tracking add-on (for full methodology refer to Appendix A).

In order to obtain representative ejection speeds, particles were tracked at various stages between 5 and 15 ms, which include the first clearly observed particles available for tracking, through to the rapidly slowing particles. Using the measured fragmentation speeds between 20 and 35 m/s, this suggests that it only takes 1 to 2 ms for the fragmentation front to propagate through the sample. This indicates that the initial particles were tracked well after fragmentation has ceased, therefore the speeds should simply be slowing with no additional influence from further fragmentation. Particles from all experiment types were tracked to indicate how different properties influence their speed. This includes the liquid water or argon experiments both performed on altered and unaltered samples with differing porosities.

3.3.4 Ballistic Analysis

Ballistic processes including speeds, travel times, and distance of travel can be estimated based on field observations and calculations using the EJECT software (version 1.4) developed by Mastin (2001). Using this software ballistic trajectories are calculated to consider a wide range of properties including fragment sizes, initial velocities, ejection angle, topography, wind, temperature, elevation, density and shape. Of these properties, results are most strongly influenced by the initial velocity, ejection angle and wind speed (Morgan et al., 2009). With no observations of pre-historic eruptions or many of the historic eruptions, calculations such as these provide a best estimate for how these eruptions may have occurred.

3.4 Discussion of Results

Detailed analysis of experimental results has already been discussed in Chapter 2. Here only those results applicable to the Okaro eruption are considered, providing an indication of processes occurring during eruption and additional details to describe the characteristics of this particular event.

3.4.1 Fragmentation Thresholds

Experimental results show fragmentation thresholds of altered ignimbrite range between 5 and 7.5 MPa (Figure 2.2). This indicates the overpressure and amount of decompression required to trigger an eruption at Okaro, otherwise known as the fragmentation threshold. In addition to this pressure, the influence of overburden needs to be considered. Based on reconstructed stratigraphy at Okaro (Figure 3.2) and an excavation depth of 100 m, the overburden pressure would be approximately 1.6 MPa. This value is relatively minor in contrast to the fragmentation threshold, fitting within the error of these values, to suggest that the influence of lithostatic load is not very significant at this location.

Comparing the results from the 300°C and room temperature experiments, suggests that temperature has only a minor influence on the fragmentation threshold. Results obtained for each temperature range fit within the error of the other. This gives confidence in our results, as the actual temperature within the geothermal system prior to fragmentation is not well constrained, likely falling somewhere between 180 and 350°C. Kueppers (2005) noted that for

experiments performed at 850°C, the fragmentation threshold is reduced with higher temperatures (Kueppers, 2005; Spieler et al., 2003). Based on the new experimental results, it is assumed that 300°C is low enough to not influence the fragmentation threshold, indicating that within typical hydrothermal systems the temperature does not play a significant role on the fragmentation threshold.

3.4.2 Fragmentation Speeds

Fragmentation speed was discussed briefly in chapter 2, noting that there appears to be only a moderate to weak correlation between fragmentation speed and level of saturation, sample type (porosity) or applied pressure. Within the Okaro setting, where the decompression required for eruption is relatively low (between 5 and 7.5), the speed at which the fragmentation front will excavate falls between 20 and 35 m/s (Figure 2.3). Within this range, the error on each measurement is very small, with a maximum variance of 1 m/s, indicating a high level of accuracy. But large scatter was found between experiments performed at the same conditions. To better constrain the range of these values, further experiments are required.

Several apparent trends exist within this data. At low pressures, such as within the Okaro eruption, liquid water experiments produce slower fragmentation speeds than equivalent argon gas experiments (Figure 2.3). In addition to this trend, it appears that altered (higher porosity) samples fragment at overall higher speeds than the equivalent unaltered material (with the exception of a few outliers). A range of fragmentation speeds should be considered, but based on results within this study (Figure 2.3) the fragmentation speed for the Okaro eruption is likely closer to the 20 m/s end of this range, as it fragmented altered ignimbrite from a liquid hydrothermal system.

3.4.3 Fragmentation Energy

Fragmentation energy is supposed to be directly related to the amount of volume change occurring from gas expansion and steam flashing. Pure gas expansion has lower volume change, in contrast to steam flashing. The temperature and pressure conditions prior to eruption at Lake Okaro suggest that the hydrothermal system was predominantly in a liquid

phase (Figure 3.5) and therefore significant expansion and energy release would occur, This produces a much larger eruption than if this was a vapour dominated system.

The amount of expansion that can occur is strongly dependent on the sample porosity. Higher porosity means the sample contains more argon or water which has a grater potential for expansion resulting in higher energy and smaller particles (Kueppers 2005; Kueppers et al., 2006). This is apparent in the grain sizes observed here (Figure 2.4). This may additionally reflect the physical properties of higher porosity samples. Higher porosity means thinner vesicle walls so that smaller particles are produced on fragmentation. Within these experiments higher porosity reflects increased alteration, which may indicate that clay weakening is occurring with the influence of liquid water (Vásárhelyi & Ván, 2006).

The relationship between the energy released during an eruption and the crater diameter has been determined from a wide range of sources including natural, nuclear and chemical eruptions. It has been suggested that this can be described with the following relationship (Sato & Taniguchi, 1997):

$$E\ (J) = 4.45x10^{6}\, D^{3.05}$$

When applied to Okaro, this suggests that $2.1x10^{15}$ J of energy was relased, assuming an average crater diameter of 700 m. This is consistant with the experimental data presented by Goto et al. (2001). With the experimentally derived energy from fragmentation experiments suggesting an energy release of 10 to 25 J/cm^3 and an estimated volume of $3.67x10^{12}$ cm^3 of erupted material (Cross, 1963; Hardy, 2005), this suggests that between $3.67x10^{13}$ and $9.17x10^{13}$ J of energy was produced at Okaro. The difference between the values suggested from the previously published relationships and our calculations differs by 2 log units, likely as a result of an understimation of the volume of material erupted from Okaro. This illustrates the significant error that can be introduced within these kinds of calculations.

3.4.4 PARTICLE EJECTION SPEEDS

To determine the particle speeds erupted from the Okaro crater, particle tracking software was used. Initial particle velocities are measured at 250 m/s, rapidly slowing with time (Figure 3.6), in a non linear trend as shown by Alatorre-Ibarguengoitia (2010). Speeds drop rapidly from greater than 250 m/s at 0.004 s after fragmentation, to below 100 m/s by 0.008 s. After

measuring ejection speeds for all 300°C experiments, these speeds appear to be independent of experiment type (steam flashing versus argon gas expansion) or sample material (altered 40% porosity versus unaltered 24% porosity). This indicates that particle speed is not influenced by energy source, alteration or porosity. In order to check repeatability, tracking was repeated providing almost identical results. This shows a maximum variation of 8 m/s thereby forming a 3.2% margin of error on these results.

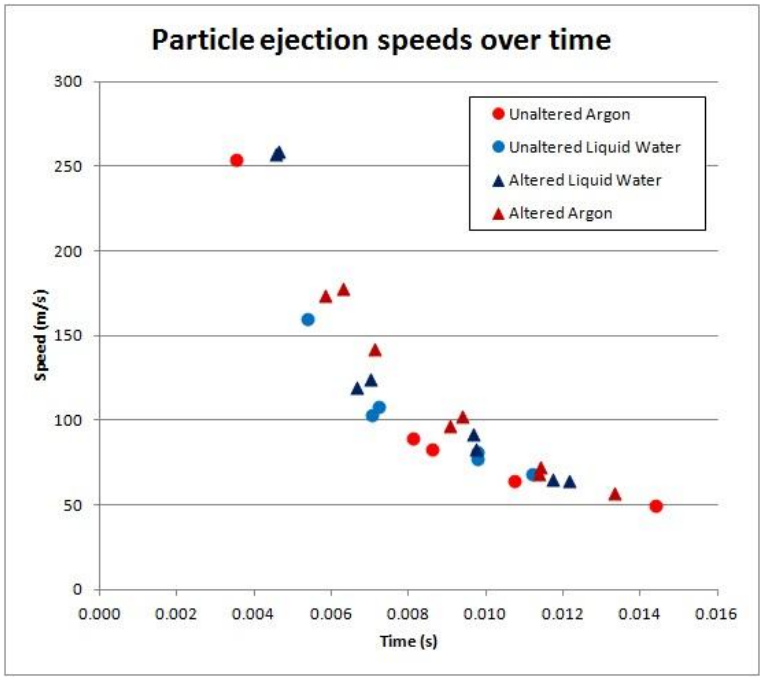

Figure 3.6: Results of particle tracking, showing the rate at which particles are ejected following initial fragmentation. Although all results match closely, note that the most representative of the Okaro eruption is the altered liquid water experiment (as the eruption was predominantly through altered material from a liquid phase hydrothermal system), shown here by the blue triangles.

3.4.5 BALLISTIC ANALYSIS

Blocks of altered Rangitaiki ignimbrite deposited near the shore of Lake Okaro, approximately 440 m from the inferred vent location, show average clast sizes between 0.1 and 0.2 m. Using EJECT (Mastin, 2001), a range of initial velocities were tested to determine the likely ejection angles, vertical heights, final velocities and travel times.

In order to reach the observed distances for ballistics between 0.1 and 0.2 m from source, with a maximum initial velocity of 250 m/s, ballistics would have an ejection angle of between 85° and 87°. Calculated values suggest that these clasts would travel an average of 395 m from source, reaching maximum heights between 1591 and 2076 m (relative to ejection angle), with final velocities ranging between 134 and 167 m/s, to give a total travel time between 36 and 41 s.

It is highly unlikely that within the Okaro eruption any clasts were ejected at the maximum speed of 250 m/s, as a significant portion of this velocity would be lost to crater formation and initial explosion processes. To compensate for these factors, EJECT was also used to calculate eruption scenarios with initial velocities of 200, 150 and 100 m/s, as illustrated in the table below. This illustrates the high level of variability that can occur within these eruptions, simply as a result of different ejection velocities.

Initial velocity (m/s)	Distance travelled	Ejection Angle	Vertical Height (m)	Final Velocity (m/s)	Travel Time (s)
200	407	84	1205	123	31.4
150	430	81	796	108	25.5
100	411	74	395	83	18.0

Within natural systems, such as Okaro, there is likely to be significant variation in eruption characteristics. It is most likely that a range of initial velocities would have occurred from the Okaro crater. From the calculations described above, this indicates that the Okaro eruption would most likely include ballistics ejected at angles between 74 and 84°, which reach a wide range of heights up to 1200 m, with final velocities up to 123 m/s resulting in travel times up to 31 s. These calculations all assume a scenario with no wind as this has little influence on ballistics. The range of results described here acts to highlight the error involved with this method. Without better constraints, significant variability will exist within the calculated results.

3.5 DISCUSSION OF OKARO ERUPTION MODEL

Applying both field observations and experimentally derived parameters to the eruption of Lake Okaro, allows a model of eruption processes to be established. A possible scenario for how this eruption occurred is illustrated in Figure 3.7. With very few in depth eruption studies existing, this represents one of the first models to describe a hydrothermal eruption as determined from a range of field observations, experimental and mathematical modelling.

Figure 3.7 a, describes the Okaro area prior to fragmentation. This illustrates the local stratigraphy (Figure 3.2), the measured properties of major units and the hydrothermal system itself which extends through the siltstone and well into the Rangitaiki ignimbrite. The size of the hydrothermal system is inferred from the presence of alteration on all ignimbrite clasts found within breccia; indicating that the hydrothermal system extended through most if not all of the ignimbrite. Directly above the hydrothermal system a silica cap formed, as indicated by the presence silica fragments within the breccia. This would have helped contain heat and pressure within the system, pushing it closer to the point of fragmentation. With a significant thickness of material above the hydrothermal system this additionally acts to increase the pressure as a result of lithostatic load, which here is calculated as 1.6 MPa.

Based on the experimentally derived pressures (5 to 7.5 MPa) and indicated temperatures (over 180°C, as indicated by alteration assemblages) the hydrothermal system would have been in a liquid phase prior to eruption (Figure 3.5). This was heated and pressurised by the intrusion of a dyke associated with the Kaharoa phase of eruptions from Mount Tarawera (Nairn et al., 2004). This would have increased temperatures to well above 180°C, much likely closer to 300°C, priming the system so that only a small trigger was required to initiate the eruption.

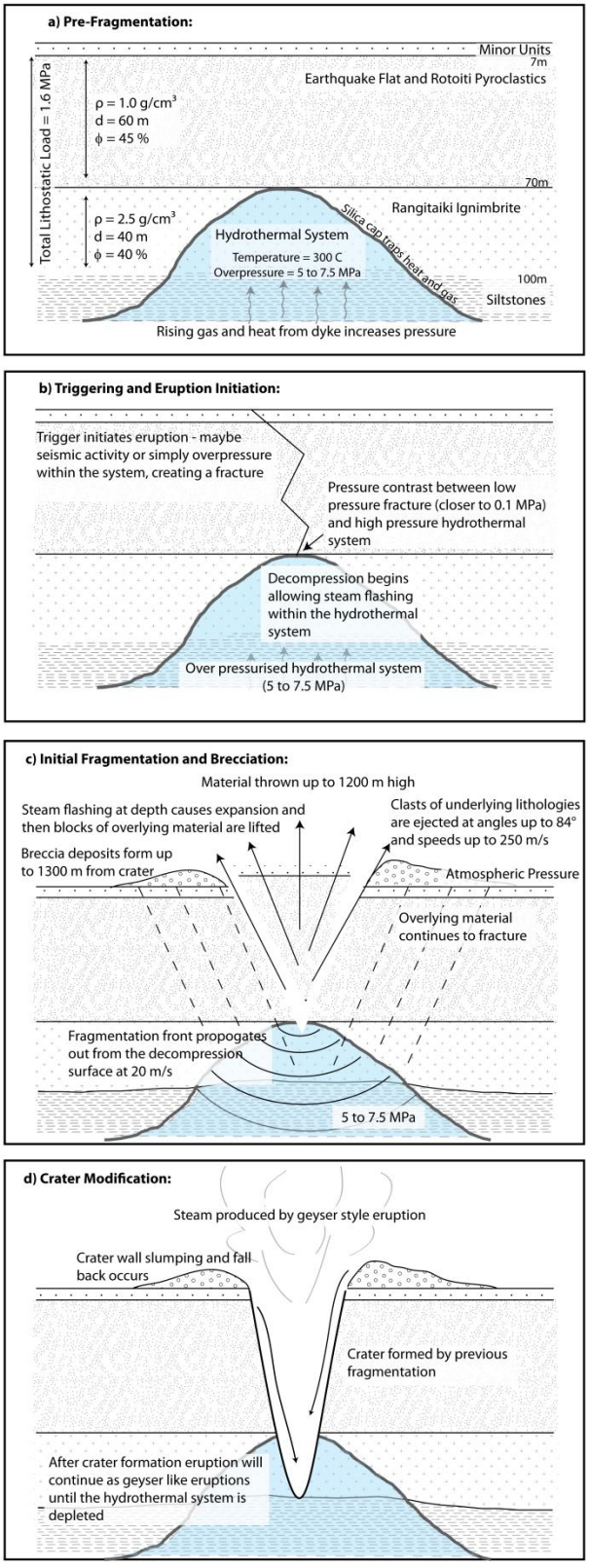

Figure 3.7: The series of events that occurred prior to and during the eruption forming Lake Okaro.

Figure 3.7 b, shows the hydrothermal system when fragmentation triggering occurs. Although this model does not illustrate a specific eruption trigger, there are many possible triggers that could have occurred, some more likely than others. In many hydrothermal eruptions, seismic activity is suggested as the most common trigger (Barberi et al., 1992; Bixley & Browne, 1988; Browne & Lawless, 2001; Smith, 2000), which would be appropriate for the Lake Okaro eruption, with the Ngapouri fault nearby. A recent study by Seebeck (2009), has shown that within the Okataina region fault movement occurs independently from dyke intrusion, proving that a dyke most likely intruded and primed the system, while an independent seismic event later triggered the eruption. With an overpressure between 5 and 7.5 MPa and an overburden of 1.6 MPa, this adds additional evidence to suggest that the eruption was triggered by fault motion rather than just overpressure build up and weakening of the overlying material from clay alteration (Morgan et al., 2009), as significant decompression is required.

The trigger would create a fracture pathway to the surface, increasing permeability (Fontaine et al., 2003) and allowing decompression to begin from the highly over-pressurised region within the hydrothermal system to the atmospheric pressures at the surface. Within the fracture itself a pressure differential exists between the low (almost atmospheric pressure) within the fracture and the pressurised system around it. The interface between the low pressure fracture system and the high pressure hydrothermal system allows decompression to occur. At this point water within the hydrothermal system begins to flash to steam, significantly increasing in volume; therefore shattering and lifting the overlying rock if sufficient amounts of decompression occur (Figure 3.7 c). After the initial blast, the fragmentation front would continue to propagate outwards and further down into the hydrothermal system, with a more top-down style mechanism. Experimental results suggest that this would move at a speed of 20 m/s, indicating that only a few seconds would be required to excavate to the maximum depth. Following the initial blast and further propagation of the fragmentation front, it is likely that continued steam an geyser style eruptions would continue on for a time, until the hydrothermal system is depleted (Fontaine et al., 2003).

As these are violent eruptions, material may be erupted before falling back into the crater to then be re-erupted several times (Figure 3.7 d). Ballistic modelling (Mastin, 2001) suggests that average 0.1 to 0.2 m sized clasts would be thrown up to 1200 m into the air, travelling

with a final velocity between 123 and 83 m/s for a maximum of 31 s before landing. As a result of the liquid phase hydrothermal system and higher associated energy, smaller particles are produced; with both field observations and modelling suggest that traces of breccia can be found as much as 1300 m from source. This indicates that the ejection angle is highly variable, likely less than 84°, while also suggesting much greater variability in travel times and velocities. With crater development there will be slumping of the walls as more fragmentation occurs, prompting this additional material to be ejected, all of which act to produce the poorly sorted breccia deposits seen today. Overall this data reinforces that this is a moderate sized eruption, representative of the type 5 style as discussed in Chapter 1.

Based on the presence of hot and in some cases boiling or superheated geothermal fluids that are currently observed around the lake (MacFarlan, 1990), this suggests that there is potential within the system for future eruptions. The chances of another eruption of this scale are relatively minor as it would require something to prime the system (such as renewed magmatic activity at Mt Tarawera) in addition to a significant trigger (for instance movement on the Ngapouri fault). The large uncertainty involved in both of these factors reinforces the need for better understanding of these systems, to help begin to eliminate the hazards and associated risks.

3.6 FUTURE WORK

With any research the more you begin to understand the more questions that develop. This leaves plenty of scope for future work. To improve upon these experiments, the first step is to test a wider range of sample materials. Results obtained within this study indicate that alteration and therefore porosity play a significant role in many fragmentation parameters, so testing a moderate or highly altered ignimbrite would provide a better indication of this influence. In addition to testing different alteration levels, it would be interesting to test different rock types such as the more pumiceous earthquake flat pyroclastics or mud/siltstones.

After a greater range of sample types have been selected the next step is to check the influence that saturation and heating has on samples themselves. Does either of these change the porosity, permeability, rock strength, surface area or size? This must be investigated in order to validate the results of the other experimentally derived parameters.

Rock strength is influenced by the water content within sandstones (Vásárhelyi & Ván, 2006), so further studies should investigate the influence that this has on the different sample materials. This would provide additional evidence that the observed processes are actual phenomena, rather than just weakening as a result of saturation.

Ideally a method in which to determine the fragmentation threshold for liquid water saturated samples should be developed. Here it is assumed that the threshold remains the same whether the experiment is run with argon gas or liquid water. Through testing the liquid water fragmentation threshold and determining if this assumption is true, will provide greater confidence in the eruption model and ability to estimate the amount of decompression required for eruption from any particular system.

Within this experimental set up, fragmentation occurs following the top down mechanism, while in the eruption model a combination of bottom up and top down eruption styles are described. This model does not take into account the amount of energy required to lift the overlying rock material, allowing further fragmentation to occur in a more top down manner. This should be investigated to quantify how the amount of energy lost to ejecting material influences the eruption processes.

The energy required to lift overlying material also relates to the initial amount of decompression that is required to allow enough steam flashing to trigger an eruption. With only minor decompression from a small fracture, a tiny portion of the hydrothermal system will flash to steam. If there is a significant pathway for decompression gas will escape rapidly allowing further flashing and fragmentation. If the decompression pathway isn't great enough, a portion of the hydrothermal system will flash to steam, pressurising the immediate zone around before gradually degassing, with this cycle repeating again and again. The size and geometry of the fracture pathways should be investigated and quantified to determine how this influences steam flashing and eruption.

3.7 CONCLUSION

Within this study both experimental techniques and field observations have been applied, to produce a model describing a possible scenario for the eruption forming Lake Okaro. This method enables experimentally derived parameters such as fragmentation pressures,

velocities, energy and the resultant grain sizes to be understood in the context of an actual eruption, providing the following key points:

- In order for an eruption to occur at Lake Okaro, between 5 and 7.5 MPa of over pressure is required.
- On decompression, an eruption would occur with the fragmentation front propagating outwards at speeds between 20 and 35 m/s.
- Coming from a liquid phase hydrothermal system, significant energy is produced thereby creating small particle sizes – significantly smaller than that of an equivalent eruption from a vapour phase system.
- Initial ballistic velocities are approximately 250 m/s, reducing rapidly with time.
- Calculations suggest that during the eruption particles were ejected at a range of angles from 78° to 84°, reducing as wind speed increases.
- In order for ballistics between 0.1 and 0.2 m in diameter to reach of distance of 440 m from the crater this assumes a travel time of up to 31 s with speeds up to 123 m/s.
- These processes work together to create the 700 m wide Okaro crater that is still present today.

Although this provides what is currently the most likely eruption scenario, future work will enable greater confidence in this model. As these eruptions are still highly unpredictable, it is important that further research is completed with this technique and other complimentary methods, to enable a greater understanding of how these eruptions operate. Only when they are better understood, will it be possible to possible to mitigate their associated hazards and reduce the risks to society, industry and the natural environment.

Chapter Four

Summary

Results presented within this thesis provide additional information and new perspectives on many different fields of geology. This includes experimental volcanology, physical volcanology, hazards, and geothermal research.

The models presented here represent the cumulative results of this research. Firstly sample material was characterised, fragmentation parameters measured and grain size distributions were obtained for each eruption type, overall allowing the creation of a well constrained eruption model. Not only does this improve understanding of general hydrothermal and phreatic eruptions, but it allows for improved hazard modelling for Taupo Volcanic Zone eruptions like the Okaro eruption. The following is a summary of the key results from my research.

- This study represents the first shock tube experiments of this kind performed on natural ignimbrite samples and is one of the first ever performed on natural clastic material.
- Although many studies have been performed with the Alidibirov and Dingwell's (1996) fragmentation bomb, this experimental study represents one of the first phreatic and hydrothermal fragmentation studies performed with this device.
- Grain size distributions obtained, provide a measure of fragmentation efficiency involved with phreatic and hydrothermal fragmentation, while providing measured grain sizes that can be applied to future ash fall distribution maps and hazard modelling.

- Combing threshold results with estimates of hydrothermal system overpressure will help establish best practices for the geothermal industry, in order to avoid triggering these eruptions while drilling.
- The higher energy and resultant smaller grain sizes produced within phreatic systems provides detail on one end of the continuum between pure phreatic and pure magmatic eruptions. This can help to better constrain phreatomagmatic eruptions which involve both magma and water, falling between the two end members.
- The case study of Lake Okaro represents one of the first hydrothermal eruption studies to combine both field observations with experimental modelling in order to develop a comprehensive eruption model.
- Details on the Lake Okaro study presented here, help to better constrain the eruptive history and model presented by Hardy (2005). This model can then be applied to other similar eruptions within the Waiotapu region, helping to better constrain the geological history of this region.

References

Alatorre-Ibarguengoitia, M., Scheu, B. & Dingwell, D., 2011. Influence of the fragmentation processes on the dynamics of Vulcanian eruptions: An experimental approach. *Earth and Planetary Science Letters,* **302**: 51-59

Alatorre-Ibarguengoitia, M., Scheu, B., Dingwell, D., Delagado-Granados, H. & Taddeucci, J., 2010. Energy consumption by magmatic fragmentation and pyroclast ejection during Vulcanian eruptions. *Earth and Planetary Science Letters,* **291**: 60-69

Alidibirov, M. & Dingwell, D., 1996. An experimental facility for the investigation of magma fragmentation by rapid decompression. *Bulletin of Volcanology,* **58**: 411-416

Alidibirov, M. & Dingwell, D., 2000. Three fragmentation mechanisms for highly viscous magma under rapid decompression. *Journal of Volcanology and Geothermal Research,* **100**: 413-421.

Barberi, F., Bertagnini, A., Landi, P. & Principe., C. 1992. A review on phreatic eruptions and their precursors. *Journal of Volcanology and Geothermal Research,* **52**: 231-246.

Baud, P. & Zhu, W., 2000. Failure mode and weakening effect of water on sandstone. *Journal of geophysical research,* **105 (B7)**: 16,371-16,389.

Bixley, P. & Browne, P., 1988. Hydrothermal eruption potential in geothermal development. *Proceedings of the 10th New Zealand Geothermal Workshop,* 195-198.

Bromley, C., 2003. Practical methods of minimizing or mitigating environmental effects from integrated geothermal developments: recent examples from New Zealand. *International Geothermal Conference,* 26-32.

Bromley, C. & Mongillo, M., 1994. Hydrothermal eruptions – A hazard assessment. *Proceedings of the 16th New Zealand Geothermal Workshop,* 45-50.

Brostow, W., 2007 Mechanical properties. *In:* Mark, J., (Ed). *Physical properties of polymers handbook,* Springer. Pp 1076.

Browne, P. & Lawless, J., 2001. Characteristics of hydrothermal eruptions, with examples from New Zealand and elsewhere. *Earth-Science Reviews,* **52**: 229-331.

Buttinelli, M., Rita, D., Cremisini, C. & Cimarelli, C., 2011. Deep explosive focal depths during marr forming magmatic-hydrothermal eruptions: Baccano Crater, Central Italy. *Bulletin of Volcanology,* **73 (7)**: 899-915.

Christenson, B., 2000. Geochemistry of fluids associated with the 1995-1996 eruption of Mt. Ruapehu, New Zealand: signatures and processes in the magmatic-hydrothermal system. *Journal of volcanology and geothermal research,* **97**: 1-30.

Cobbing, J. & Dochartaigh, B., 2007. Hydrofracturing water boreholes in hard rock aquifers in Scotland. *Quarterly Journal of Engineering Geology and Hydrogeology,* **40**: 181-186.

Cole, J., Thordarson, T. & Burt, R., 2000. Magma origin and evolution of White Island (Whakaari) volcano, Bay of Plenty, New Zealand. *Journal of Petrology,* **41 (6)**: 867-895.

Collar, R. & Browne, P., 1985. Hydrothermal eruptions at the Rotokawa geothermal field, Taupo Volcanic Zone, New Zealand. *Proceedings of the 7th New Zealand Geothermal Workshop,* 171-175.

Cronin, J., Winters, K. & Rangiheuea, A., 2006. Lake Okaro Action Plan. *Environment Bay of Plenty, Rotorua District Council, Te Arawa Maori Trust Board.*

Cronin, S., Neall, V., Lecointre, J., Hedley, M. & Loganathan, P., 2003. Environmental hazards of fluoride in volcanic ash: a case study from Ruapehu volcano, New Zealand. *Journal of Volcanology and Geothermal Research.* **121**: 271-291.

Cross, D., 1963. Soils and geology of some hydrothermal eruptions in the Waiotapu district. *New Zealand Journal of Geology and Geophysics,* **6**: 70-87.

Dellino, P., Dioguardi, F., Zimanowski, B., Buttner, R., Mele, D., La Volpe, L., Sulpizio, R., Doronzo, D., Sonder, I., Bonasia, R., Calvari, S. & Marotta, E., 2010. Conduit flow experiments help constraining the regime of explosive eruptions. *Journal of Geophysical Research,* **115**: 1-17.

Doherty, A., 2009. Blue-sky eruptions, do they exist? Implications for monitoring New Zealand's Volcanoes. Unpublished MSc thesis, University of Canterbury, Christchurch, New Zealand.

Fontaine, F., Rabinowicz, M. & Boulegue, J., 2003. Hydrothermal processes at Milos Island (Greek Cyclades) and the mechanisms of compaction-induced phreatic eruptions. *Earth and Planetary Science Letters,* **210**: 17-33.

Fowler, A., Scheu, B., Lee, W. & Mcguinness, M., 2009. A theoretical model of the explosive fragmentation of vesicular magma. *Proceedings of the Royal Society A: Mathematical, Physical and Engineering Sciences,* 1-22.

Fullard, L., 2011. Modelling the initiation of a hydrothermal eruption – the shock tube model. Unpublished PhD thesis, Massey University, Manawatu, New Zealand.

Germanovich, L. & Lowell, R., 1995. The mechanism of phreatic eruptions. *Journal of Geophysical Research,* **100 (B5)**: 8417-8434.

Google Inc., 2011. Google Earth.

Goto, A., Taniguchi, H. & Yosgida, M., 2001. Effects of explosion energy and depth to the formation of blast waver and crater: Field explosion experiment for the understanding of volcanic explosion. *Geophysical Research Letters,* **28 (22)**: 4287-4290.

Handal, S. & Barrios, L., 2004. Hydrothermal eruptions in El Salvador. *In* Rose, W., Bommer, J., Lopez, D., Carr, M. & Major, J. (Eds), *Natural Hazards in El Salvador,* Geological Society of America. Pp 245-256.

Hardy, L., 2005. Lake Okaro: Explosions and erosion – A study into erosion on the hills to the north of Lake Okaro and the 0.7 ka phreatic and hydrothermal eruptions at Lake Okaro to help understand the current geomorphology. Unpublished BSc Hons thesis, University of Otago, Dunedin, New Zealand.

Hedenquist, J. & Henley, R., 1985. Hydrothermal eruptions in the Waiotapu geothermal system, New Zealand: their origin, associated breccias, and relation to precious metal mineralization. *Geology*, **80**: 1640-1668.

Houghton, B., 1991. The 1976-1982 strombolian and phreatomagmatic eruptions of White Island, New Zealand: eruptive and depositional mechanisms at a "wet" volcano. *Bulletin of Volcanology,* **54**: 25-49.

Irwin, J., 1974. Lake Okaro and Lake Ngapouri provisional bathymetry: New Zealand Oceanographic Institute Chart, Lake Series 1:3168. *New Zealand Oceanographic Institute.*

Kigour, G., Pasqua, F., Hodgson, K & Jolly, G., 2010. The 25 September 2007 eruption of Mount Ruapehu, New Zealand: directed ballistics, surtseyan jets, and ice-slurry lahars. *Journal of Volcanology and Geothermal Research,* **191**: 1-14.

Koyaguchi, T., Scheu, B., Mitani, N. & Melnik, O., 2008. A fragmentation criterion for highly viscous bubbly magmas estimated from shock tube experiments. *Journal of Volcanology and Geothermal Research,* **178**: 58-71.

Kueppers, U., 2005. Nature and efficiency of pyroclast generation from porous magma: Insights from field investigations and laboratory experiments. Unpublished PhD thesis, Ludwig-Maximilians-Universitat, Munich, Germany.

Kueppers, U., Perugini, D. & Dingwell, D., 2006. "Explosive energy" during volcanic eruptions from fractal analysis of pyroclasts. *Earth and Planetary Science Letters,* **248**: 800-807.

Kueppers, U., Scheu, B., Spieler, O. & Dingwell, D., 2006. Fragmentation efficiency of explosive volcanic eruptions: A study of experimentally generated pyroclasts. *Journal of Volcanology and Geothermal Research,* **153**: 125-135.

MacFarlan, D., 1990. PL 31-1788 Lake Okaro Technical Report. *Ministry of Economic Development, New Zealand.* Pp 17.

Martel, C., Dingwell, D., Spieler, O., Pichavant, M. & Wilke, M., 2000. Fragmentation of foamed silicic melts: an experimental study. *Earth and Planetary Science Letters,* **178**: 47-58.

Mastin, L., 1995. Thermodynamics of gas and steam-blast eruptions. *Bulletin of Volcanology,* **57**: 85-98.

Mastin, L., 2001. A simple calculator of ballistic trajectories for blocks ejected during volcanic eruptions. Pp 18.

Mcguinness, M., Fowler, A., Scheu, B. & Lee, W., 2009. Exploding rocks. *International Conference on Numerical Analysis and Applied Mathematics, p*p 4.

Milicich, S. & Reeves, R., 2009. Thermal features of the Ngatamariki geothermal field. *GNS Science Consultancy Report 2009/97.* Pp 62.

Molloy, C., Shane, P. & Nairn, I., 2008. Pre-eruption thermal rejuvenation and stirring of a partly crystalline rhyolite pluton revealed by the Earthquake Flat Pyroclastics deposits, New Zealand. *Journal of the Geological Society,* **165:** 435-447.

Montalto, A., 1995. Seismic assessment of phreatic-explosion hazard at "La Fossa" volcano (Island of Vulcano, Italy). *Natural Hazards,* **11**: 57-73.

Mordret, A., Jolly, A., Duputel, Z. & Fournier, N., 2010. Monitoring of phreatic eruptions using interferometry on retrieved cross-correlation function from ambient seismic noise: results from Mt. Ruapehu, New Zealand. *Journal of Volcanology and Geothermal Research,* **191:** 46-59.

Morgan, L., Shanks, W. & Pierce, K., 2009. Hydrothermal processes above the Yellowstone magma chamber; large hydrothermal systems and large hydrothermal explosions. *Geological Society of America,* **178**: 45-58.

Mueller, S., Scheu, B., Spieler, O. & Dingwell, D., 2008. Permeability control on magma fragmentation. *Geology,* **36 (5)**: 399-402.

Muffler, L., White, D. & Truesdell, A., 1971. Hydrothermal explosion craters in Yellowstone National Park. *Geological Society of America Bulletin,* **82**: 723-740.

Nairn, I., 1984. Stratigraphic drillholes at Rarewhakaaitu. Unpublished report.

Nairn, I., 2003. Stratigraphy of water supply well drilled at Lake Okaro in November 2003. Unpublished report.

Nairn, I., Hedenquist, J., Villamor, P., Berryman, K. & Shane, P., 2004. The ~AD1315 Tarawera and Waiotapu eruptions, New Zealand: contemporaneous rhyolite and hydrothermal eruptions driven by an arrested basalt dyke system? *Bulletin of Volcanology,* **67**: 186-193.

Nairn, I., Shane, P., Cole, J., Leonard, G., Self, S. & Pearson, N., 2004. Rhyolite magma processes of the ~AD1315 Kaharoa eruption episode, Tarawera volcano, New Zealand. *Journal of Volcanology and Geothermal Research,* **131**: 265-294.

Nelson, C. & Giles, D., 1985. Hydrothermal eruption mechanisms and hot spring gold deposits. *Economic Geology,* **80**: 1633-1639.

Nogami, K., Hirabayshi, J., Ohba, T. & Yoshiike, Y., 2000. The 1997 phreatic eruption of Akita-Yakeyma volcano, northeast Japan: Insights into the hydrothermal processes. *Earth Planets Space,* **52**: 229-236.

O'Brien, J., 2010. Hydrogeochemical characteristics of the Ngatamariki geothermal field and a comparison with the Orakei Korako thermal area, Taupo Volcanic Zone, New Zealand. Unpublished MSc thesis, University of Canterbury, Christchurch, New Zealand.

Pochee, A., 2010. Mass transfer and hydrothermal alteration in the Rotokawa Andesite, Rotokawa geothermal field, New Zealand. Unpublished MSc thesis, University of Auckland, Auckland, New Zealand.

Reyes, A., 1990. Petrology of Philippine geothermal systems and the application of alteration mineralogy to their assessment. *Journal of Volcanology and Geothermal Research,* **43**: 279-309.

Sato, H. & Taniguchi, H., 1997. Relationship between crater size and ejecta volume of recent magmatic and phreato-magmatic eruptions: Implications for energy partitioning. *Geophysical Research Letters,* **24(3)**: 205-208.

Scheu, B., Serr, F. & Dingwell, D., 2012. The influence of explosive boiling on the fragmentation behaviour of rocks: An experimental approach to phreatic and hydrothermal explosions. In publication.

Scheu, B., Spieler, O. & Dingwell, D., 2006. Dynamics of explosive volcanism at Unzen volcano: an experimental contribution. *Bulletin of Volcanology,* **69**: 175-187.

Scheu, B. & Dingwell, D., 2010. Phreatic and hydrothermal explosions: A laboratory approach. *American Geophysical Union, Fall Meeting.*

Scheu, B., Kueppers, U., Muller, S., Spieler, O. & Dingwell, D., 2008. Experimental volcanology on eruptive products of Unzen volcano. *Journal of Volcanology and Geothermal Research,* **175**: 110-119.

Scott, B. & Cody, A., 2000. Response of the Rotorua geothermal system to exploitation and varying management regimes. *Geothermics,* **29**: 573-592.

Scott, B., Gordon, D. & Cody, A., 2005. Recovery of the Rotorua geothermal field, New Zealand: Progress, issues and consequences. *Geothermics,* **34**: 159-183.

Seebeck, H. & Nicol, A., 2009. Dike intrusion and displacement accumulation at the intersection of the Okataina Volcanic Centre and Paeroa Fault zone, Taupo Rift, New Zealand. *Tectonophysics,* **475**: 575-585.

Serr, F., 2010. Fragmentation behaviour of gas and water vapur explosions. Unpublished Bachelor thesis, Ludwig-Maximilians-Universitat, Munich, Germany.

Sheridan, M. & Wohletz, K., 1983. Hydrovolcanism: Basic considerations and review. *Journal of Volcanology and Geothermal Research,* **17**: 1-29.

Simmons, S., Browne, P. & Scott, B., 2004. Field trip 2: Geothermal systems. *26th New Zealand Geothermal Workshop.* Pp 32.

Smith, T., 2000. Mathematical modelling of underground flow processes in hydrothermal eruptions. Unpublished PhD thesis, Massey University, Manawatu, New Zealand.

Smith, T. & McKibbin, R., 2000. An investigation of boiling processes in hydrothermal eruptions. *Proceedings of the World Geothermal Congress 2000,* **1**: 699-704.

Speed, J., Shane, P. & Nairn, I., 2002. Volcanic stratigraphy and phase chemistry of the 11 900 yr BP Waiohau eruptive episode, Tarawera Volcanic Complex, New Zealand. *New Zealand Journal of Geology and Geophysics,* **45(3)**: 395-410.

Spieler, O., Alidibirov, M. & Dingwell, D., 2003. Grain size characteristics of experimental pyroclasts of the 1980 Mount St Helens cryptodome dacite: effects of pressure drop and temperature. *Bulletin of Volcanology,* **65**: 90-104.

Spieler, O., Dingwell, D. & Alidibirov, M., 2004. Magma fragmentation speed: an experimental determination. *Journal of Volcanology and Geothermal Research,* **129**: 109-123.

Spieler, O., Kennedy, B., Kueppers, U., Dingwell, D., Scheu, B. & Taddeucci, J., 2004. The fragmentation threshold of pyroclastic rocks. *Earth and Planetary Science Letters,* **226**: 139-148.

Srodon, J. & Eberl, D., 1984. Illite. *In* Reviews in Mineralogy, Volume 13: Micas. *Mineralogical Society of America.* Pp 495-543.

Thiery, R. & Mercury, L., 2009. Explosive properties of water in volcanic and hydrothermal systems. *Journal of Geophysical Research,* **114(B5)**: 1-19.

Vasarhelyi, B. & Van, P., 2006. Influence of water content of the strength of rock. *Engineering Geology,* **84**: 70-74.

Walker, G. & Wilson, C., 1983. Lateral variations in the Taupo ignimbrite. *Journal of Volcanology and Geothermal Research,* **18**: 117-133.

White, D., Muffler, L. & Truesdell, A., 1971. Vapour-dominated hydrothermal systems compared with hot-water systems. *Economic Geology*, **66**: 75-97.

Wilson, C. & Walker, G., 1985. The Taupo eruption, New Zealand I. General aspects. *Philosophical Transactions of the Royal Society of London, Series A, Mathematical and Physical Sciences,* **314 (1529)**: 199-228.

Wohletz, K., 1983. Mechanisms of hydrovolcanic pyroclast formation: Grain size, scanning electron microscopy and experimental studies. *Journal of Volcanology and Geothermal Research,* **17**: 31-63.

Appendix A

Experimental Fragmentation: Background and Methodology

Experimental Fragmentation

Background

The field of experimental fragmentation has grown significantly since the development of the "fragmentation bomb" shock tube device, developed by Alidibirov and Dingwell (1996). This technique has focused exclusively on magmatic systems, with no previously published studies of phreatic or hydrothermal fragmentation. Techniques for magmatic systems can be applied to phreatic systems with only minor changes required. The advantage of the fragmentation bomb is that it enables repeated experiments on natural samples to easily test the influence of a wide variety of natural characteristics such as chemistry, crystallinity and vesicularity (Spieler et al., 2004). Using the fragmentation bomb it is possible to constrain the effects that these characteristics have on the fragmentation process.

Fragmentation Mechanisms

Three different mechanisms have been identified to describe how fragmentation occurs (Alidibirov & Dingwell, 2000). These are referred to as 1) unloading via an elastic wave, 2) layer by layer fragmentation and 3) gas filtration. The first mechanism occurs when rapid decompression creates an elastic wave. This wave propagates downwards creating fractures parallel to the wave front, which are forced open through decompression to produce fragmentation. The second mechanism (layer by layer fragmentation) occurs when decompression is slightly slower and an elastic wave does not form. Gas expansion within the vesicles near the decompressed surface causes small layers to break off as the fragmentation

front propagates through the rock. Finally the last method, gas filtration, occurs when sample permeability is high enough that degassing creates a pressure gradient within the sample thereby triggering fragmentation. If this pressure gradient is not high enough, pure degassing will occur with no fragmentation (Mueller et al., 2008).

Although layer by layer fragmentation is thought to be the most common mechanism by which fragmentation occurs, it is also possible for a combination of two or even all three of these mechanisms to occur depending on the rock properties and rate of decompression (Alidibirov & Dingwell, 1996). Within the experiments described here, layer by layer fragmentation has been identified as the main driver of fragmentation, based on the "plate" like fragments that form (Martel et al., 2000).

Fragmentation Bomb Set-Up

In order to test the key properties influencing fragmentation, including temperatures, pressure and rates of decompression (Kueppers et al., 2006), a device commonly known as the fragmentation "bomb" was used. This is made up of a modified shock tube. The simplest shock tube is composed of a tube where two separate chambers (at high and low pressures respectively) are separated by a diaphragm (Fullard, 2011). As with the shock tube set up, there are three main components to the bomb; the pressurised autoclave, the diaphragms and the large tank where fragmented material is caught (Figure 2.1).

The lower section of the bomb forms the autoclave which holds the sample prior to fragmentation, allowing it to be heated and pressurised to represent conditions within a natural hydrothermal system. A thermocouple, in addition to both static and dynamic pressure sensors are used to accurately record these conditions. Using different autoclaves developed from a range of metals, a wide variety of pressures and temperatures can be achieved. Directly above the autoclave is a series of two diaphragms, controlling the pressure at which fragmentation is triggered. Diaphragms are made from small metal disks (of copper, iron or aluminium), imprinted with the pattern of a circle and cross, the depth of which controls their opening pressure (Kueppers, 2005). Fragmentation occurs when the pressure differential on either side of the diaphragm becomes too great causing it to burst. Rupture of the diaphragms allows rapid decompression of the autoclave, thereby triggering sample fragmentation. Above

the diaphragms, forming the top portion of the bomb is a large tank measuring 3 m high, by 0.4 m in diameter, where the fragmented material is caught.

Running an Experiment

To run an experiment, firstly the sample (either oven dried or saturated with liquid water) is placed within the autoclave and the autoclave fully assembled. A small amount of pressure is added to check for leaks, after which the furnace is placed around the autoclave, then heated to the desired temperature (here room temperature or 300°). For the oven dried samples, pressurised with argon gas, the sample is initially heated before being pressurised. In contrast to the liquid water experiments, an additional 5 MPa of pressure is added before heating, to ensure that the sample stays within the correct pressure and temperature conditions to remain as a liquid until triggering (Figure 3.5).

To trigger an experiment, overpressure is increased by turning on the flow of argon gas to the autoclave. Then the valve between the two diaphragms is quickly opened, creating a significant pressure difference between the low pressure in the sample collection tank and the high pressure under the diaphragms, causing them to fail. The two diaphragms burst almost simultaneously allowing a decompression front to propagate down into the autoclave and through the sample itself, producing fragmentation.

Pre Fragmentation Sample Characterisation

Porosity Measurements

Prior to fragmentation all samples are measured with helium pycnometry to determine open and closed porosity. Open porosity refers to the pore space that argon gas can flow into, while closed porosity reflects the fully enclosed pores that flowing gas is unable to reach. Knowledge of sample porosity is essential for fragmentation experiments, as it is one of the parameters which shows the strongest influence on fragmentation processes (Spieler et al., 2004).

Open porosity is obtained from a solid core. This is calculated using sample volume and density from the pycnometer, which is then compared to the geometric volume (length multiplied by width) with the following formula:

$$Open\ Porosity = \frac{Geometric\ Volume\ x\ Pycnometer\ Volume}{Geometric\ Volume}\ x\ 100$$

Closed porosity is measured after milling the sample to a fine powder and then determining density with the pycnometer. It can then be calculated with the following formula:

$$Closed\ Porosity = \left[\frac{Powder\ density\ x\ Geometric\ density}{Powder\ density}\ x\ 100\right] -\ Open\ Porosity$$

Sample Saturation

Before running the liquid water experiments, a study was undertaken to determine the time required for full saturation and what the maximum achievable saturation is. Saturation refers to the proportion of pore space that is filled with water. This is determined by initially weighing an oven dried sample, before submerging it in water and placing under a vacuum. The vacuum helps remove air from the pore spaces, allowing water to be more easily absorbed. When removed from the water, the sample is lightly towel dried to remove any surface water before re-weighing. The weight difference between fully dry and fully saturated gives the amount of water that has been absorbed (in ml). Finally the difference between the pore space (ml) and the amount of water absorbed can be converted to a percentage, giving the proportion of the sample that is saturated.

Within the two sample types tested (altered and unaltered) similar trends of saturation occur. Within the first hour, saturation occurs rapidly, after which little change occurs through till 96 hours when the trial ended (Appendix Figure 1). This suggests a minimum 1 hour saturation time is sufficient.

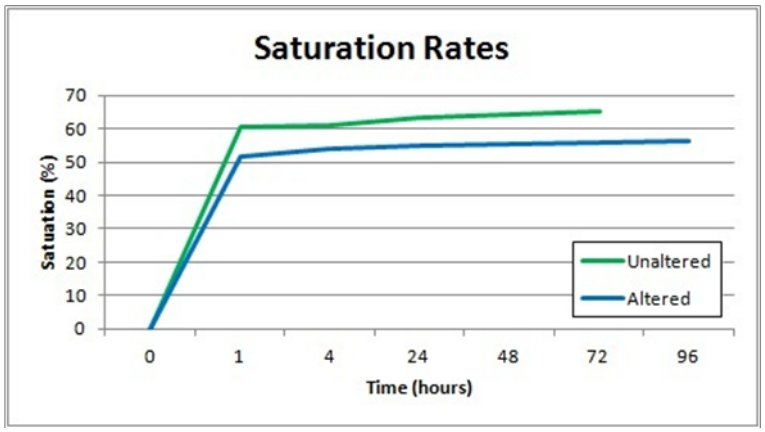

Appendix Figure 1: Rate of saturation for both altered and unaltered samples

Within these experiments a wide range of saturation values exist, ranging between 55% and apparently greater than 100% (Appendix Figure 2), this suggests significant error. Sources of this error are discussed in chapter 2. When the maximum indicated saturation is less than 100%, liquid water fragmentation experiments can still be performed, simply with a greater proportion of energy coming from gas expansion. For simplicity, all values over 100% are treated as exactly 100% and all other values as the exact calculated values, considering the error later when applying these results.

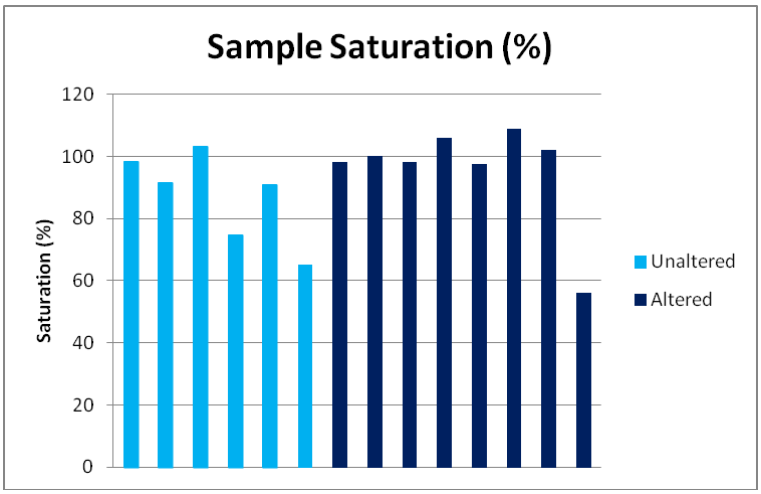

Appendix Figure 2: Saturation expressed as a percentage for all liquid water fragmentation experiments. Note the error shown where some samples register values higher than 100%.

Fragmentation Parameters

With the fragmentation bomb, there are several key parameters that can be measured. These include the fragmentation threshold, speed, velocity and post fragmentation analysis of the particles. All of which are essential to improve existing knowledge of how fragmentation occurs.

Fragmentation Threshold

The minimum pressure change required to trigger full fragmentation of a sample is known as the fragmentation threshold (Spieler et al., 2004; Kueppers et al., 2006; Scheu et al., 2008). To find this, a sample is initially subjected to low pressure differentials, the experiment triggered and the sample checked for any signs of fragmentation. The experiments are repeated, gradually increasing the applied pressure until the first signs of fragmentation occur. This is the point referred to as the fragmentation initiation pressure. The full threshold, usually 1 to 1.5 MPa higher, is when the entire sample fragments (Koyaguchi et al., 2008; Scheu et al., 2006).

As previously mentioned, fragmentation occurs when the potential energy created by the pressurised gas within the sample vesicles exceeds the tensile strength of the rock (Scheu et al., 2006; Mueller et al., 2008; Spieler et al., 2004; Fowler et al., 2009; Mcguinness et al., 2009; Alatorre-Ibargüengoitia et al., 2010). The rock strength and therefore the failure threshold is dependent on the bubble volume, wall thickness and tensile strength of the vesicle walls. Although these factors all influence the threshold, the factor with the strongest influence has been identified as sample porosity (Spieler et al., 2004; Fullard, 2011).

Fragmentation Speed

Fragmentation speed is a measure of the speed at which the fragmentation front propagates through the sample. This is measured with dynamic pressure transducers to record relative pressures above and below the sample. When the diaphragms are opened the upper pressure transducer records the pressure drop before the sample starts to fragment, while the bottom transducer reaches the same pressure after the entire sample has fragmented. Pressure drops are recorded in outputs similar to those shown in (Appendix Figure 3). From these the time

between the drop of the first signal (shown as the orange line) and the drop of the second signal (shown as the green line) can be measured. Then using simple physics with known distance and time, velocity can be calculated (Spieler et al., 2004).

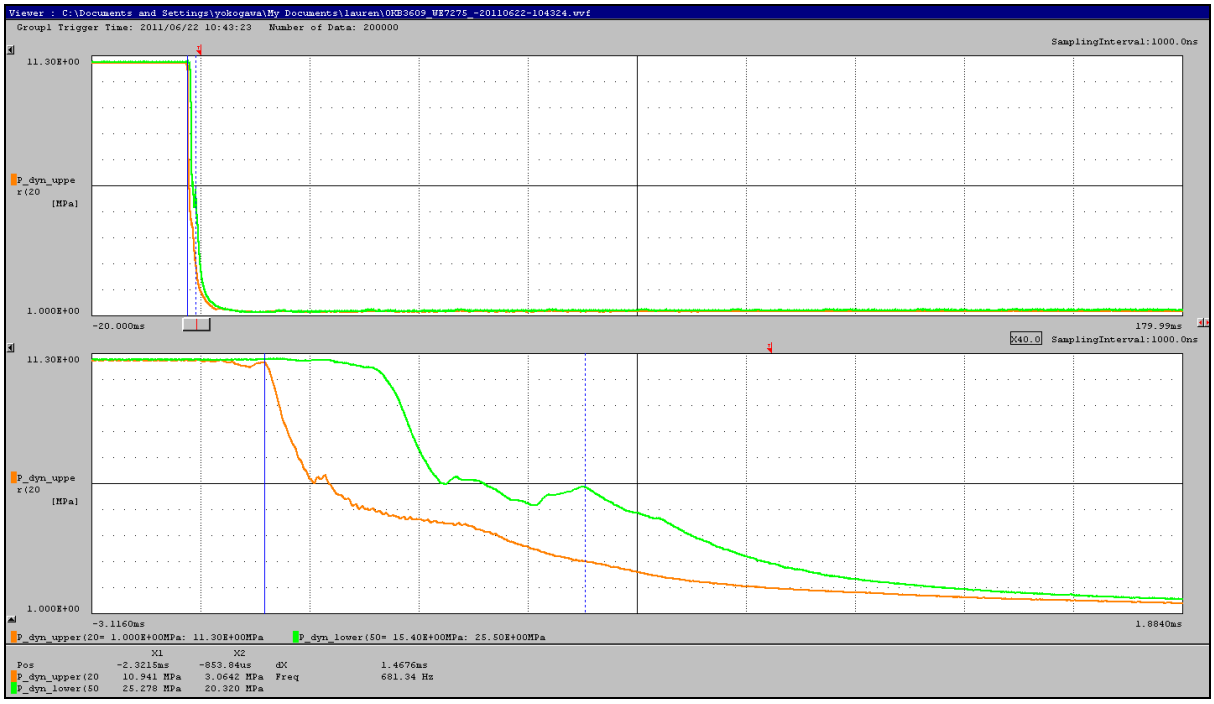

Appendix Figure 3: Pressure signals recorded from a 10 MPa argon gas experiment

PARTICLE VELOCITY

Ejection velocity of fragmented particles can be measured using two different methods. The first method uses a series of charged copper wires placed in the path of the particles. During fragmentation the particles will break the wires, cutting the circuit, causing the time to be recorded (Alatorre-Ibargüengoitia et al., 2010). Using the time along with the distance between the wires, ejection velocity can easily be calculated. The second method uses high speed camera footage to track the particles and determine their velocities (Alatorre-Ibargüengoitia et al., 2011).

Here high speed camera footage was used to determine particle velocities. The experiments were filmed at over 15,000 fps, then analysed using ImageJ software with the MTrackJ particle tracking add-on. In order to track the particles, firstly the video must be calibrated to

the software. To do this the imported video properties must be added and a scale must be set. The frame interval must be added in order for the software to calculate the rate at which the frames are moving while the scale shows the distance they travel. The easiest technique for setting the scale is to measure and set the opening of the bottom plate as 7 cm. The software then has enough information to begin tracking. To track the particles, you simply click on one, following it through at least 10 frames. After tracking, the MTrackJ software calculates the speed at which the particles are moving, using simple physics of distance multiplied by time.

Grain Size Analysis

Post fragmentation, the tank is carefully cleaned in order to retrieve the sample, for use in later grain size analysis. The tank is cleaned with high pressure (8.5 MPa) desalinated water (Kueppers et al., 2006), enabling the recovery of more than 99% of the sample. When washing the samples out of the tank, it is separated into two size fractions. This is achieved by washing the samples through a 125 micron sieve. The coarse fraction is air dried, then sieved to determine the weight percentage of each size category. The fine fraction is heated to speed up the drying process, then analysed with a Coulter LS230 for laser refraction, again to determine the weight percentage of each size.

Analysis of these grain sizes are then used to determine fragmentation efficiency, illustrating how energy influences particle generation (Kueppers, 2005). This is described by measuring the reduction in sample size after fragmentation (Scheu et al., 2006). As both sieving and laser refraction analysis has been proven to produce comparable results over the same grain sizes (Kueppers, 2005), both the larger and smaller size fractions can be directly compared without concern over differing results from different techniques.

Fragmentation Energy Calculations

To calculate the energy involved with phreatic fragmentation there are two different energy sources that should be considered. Firstly the energy that comes from argon gas expansion, and secondly the energy that comes from the liquid vapour transition (steam flashing).

Essentially the energy is controlled by the pressure and temperature conditions within the hydrothermal system, which in turn control the fluid phase prior to fragmentation.

Energy calculations use the method described by Scheu et al. (2012), based on the calculations described by Thiery and Mercury (2009) and Mastin (Mastin, 1995). Firstly to find the energy from gas expansion, the experimental pressure (MPa) is multiplied by the volume of pore space (cm^3) and then both are divided by 100 to give the energy of gas within a volume (J), as described in the formula below:

$$Energy\ from\ gas\ expansion = \frac{(Exp\ Pressure\ x\ Geometric\ Volume\ x\ Open\ Porosity)}{100}$$

To calculate the energy resulting from steam flashing, a generalised approximation of energy conversion is used. Here this is a value of 50 J/g, calculated by Thiery and Mercury (2009), based on the pressure and temperature conditions at which these experiments were run. This assumes that no additional heat was added and that the water was at its boiling point (Thiéry & Mercury, 2009). To calculate steam flashing energy (J), this approximation is combined with the volume of added water (ml = g), as shown below:

$$Energy\ from\ steam\ flashing = 50\ x\ amount\ of\ water\ added$$

Then to finally calculate the total energy per volume (J/cm^3), the energy from gas expansion and steam flashing are combined:

$$Total\ energy\ per\ volume = \frac{Energy\ from\ steam\ flashing + Energy\ from\ gas\ expansion}{Geometric\ volume}$$

Since J/cm^3 can be considered equal to MPa (Brostow, 2007), these values can be directly compared to the amount of decompression that was required to trigger this energy release.

SUMMARY

In summary, there are many different stages that go into performing fragmentation experiments and the analysis that follows. Detailed methodology was described in this section

to enable all components of these experiments to be repeated. For further details, please refer to the indicated reference material.

Appendix B

Raw Data:

Sample Name	Sample length (mm)	Connected dry porosity (%)	Pressure (MPa)	Temperature (°C)	Saturation (%)	Fragmentation?	Fragmentation Velocity (m/s)	Grain Size (phi)	Fragmentation Energy (J/cm^3)
RAN-B-02	41.6	41.6	15.0	300	98.3	full	31.4	0.5	11.8
RAN-B-03	41.2	24.1	1.0	300	0.0	none			0.2
	41.2	24.1	5.0	300	0.0	none			1.2
	41.2	24.1	4.7	300	0.0	partial			1.1
	41.2	24.1	5.9	300	0.0	partial			1.4
	41.2	24.1	8.0	300	0.0	full			1.9
RAN-B-04	41.6	24.8	3.1	300	0.0	partial			0.8
	41.6	24.8	6.0	300	0.0	partial			1.5
	41.6	24.8	7.0	300	0.0	partial			1.7
	41.6	24.8	8.0	300	0.0	partial			2.0
	41.6	24.8	9.0	300	0.0	partial			2.2
	41.6	24.8	10.0	300	0.0	partial			2.5
	41.6	24.8	12.0	300	0.0	full			3.0
RAN-B-06	40.4	23.0	5.0	300	0.0	full			1.1

Sample Name	Sample length (mm)	Connected dry porosity (%)	Pressure (MPa)	Temperature (°C)	Saturation (%)	Fragmentation?	Fragmentation Velocity (m/s)	Grain Size (phi)	Fragmentation Energy (J/cm3)
RAN-B-07	42.2	25.2	15.0	300	0.0	full		0	3.8
RAN-B-08	41.5	25.6	8.3	250	91.6	full	16.6	0.5	11.9
RAN-B-09	40.7	23.6	10.0	300	0.0	full		-0.5	2.4
RAN-B-10	42.5	24.1	15.0	300	103.3	full		0 .5	12.3
RAN-B-12	41.4	26.2	15.0	300	0.0	full	29.4	-0.5	3.9
RAN-B-14	41.6	24.6	5.0	300	0.0	partial			1.2
	41.6	24.6	6.0	300	0.0	none			1.5
	41.6	24.6	6.0	300	0.0	full			1.5
RAN-B-15	41.2	24.3	10.0	284	74.8	full	23.1	0.5	9.7
RAN-B-16	38.9	24.4	6.0	RT	0.0	partial			1.5
	38.9	24.4	7.0	RT	0.0	partial			1.7
	38.9	24.4	8.0	RT	0.0	full			2.0
RAN-B-17	40.9	25.4	15.0	300	91.1	full	33.1	0.5	11.9
RAN-B-20	41.3	26.0	10.0	300	0.0	full	18.6	0	2.6
RAN-B-21	41.1	41.4	15.0	300	0.0	full	17.0		6.2
RAN-B-22	40	23.3	4.0	RT	0.0	full			0.9
RAN-B-23	40.4	23.4	15.0	300	0.0	full	24.7	0	3.5
OKB-36-01	40.1	39.7	15.0	300	0.0	full	37.8	0	6.0
OKB-36-02	39.2	39.2	8.0	300	98.2	full		0	20.1
OKB-36-03	41.3	39.7	6.0	RT	0.0	none			2.4
	41.3	39.7	7.0	RT	0.0	full			2.8
OKB36-05	40.6	40.6	8.0	300	0.0	full	28.1	-0.5	3.2

Sample Name	Sample length (mm)	Connected dry porosity (%)	Pressure (MPa)	Temperature (°C)	Saturation (%)	Fragmentation?	Fragmentation Velocity (m/s)	Grain Size (phi)	Fragmentation Energy (J/cm3)
OKB-36-06	40.7	40.7	15.0	300	0.0	full		0	6.1
OKB-36-07	40.5	40.0	9.0	194	100.2	full	14.4	1	3.8
OKB-36-08	40.7	40.7	15.0	300	98.2	full			19.3
OKB-36-09	41.1	40.8	10.0	300	0.0	full	41.5	-0.5	4.1
OKB-36-10	39.5	38.7	10.0	300	106.1	full		0.5	19.3
OKB-36-11	41.6	39.9	15.0	300	0.0	none			6.0
	41.6	39.9	15.0	300	0.0	full	30.3	-0.5	6.0
OKB-36-12	39.6	40.2	10.0	300	0.0	full	41.1	-0.5	4.0
OKB-36-13	41.1	41.1	13.0	296	2.1	full	44.3	1	24.2
OKB-36-15	40.3	40.4	4.0	RT	0.0	partial			1.6
	40.3	40.4	5.0	RT	0.0	partial			2.0
	40.3	40.4	6.0	RT	0.0	full			2.4
OKB-36-16	41.6	41.1	15.0	300	97.4	full	38.7	1	20.2
OKB-36-17	40.3	38.3	5.0	300	0.0	full			1.9
OKB-36-18	40	40.0	8.0	287	108.8	full	19.7	0	19.4
OKB-36-19	40.3	38.5	8.0	300	0.0	full	34.2	-0.5	3.1
OKB-36-20	39.4	40.1	12.2	300	102.0	full		1	20.4
OKB-36-22	41.5	39.3	7.5	300	0.0	full			2.9
OKB-36-23	41.7	38.6	1.5	300	0.0	none			0.6